KfK 2546
März 1978

# Further Development of the LMFBR Accident Analysis Codes HOPE and KADIS: Automatic Data Transfer, New Equation of State

E. A. Fischer, G. Arnecke
Institut für Neutronenphysik und Reaktortechnik
Projekt Schneller Brüter

Kernforschungszentrum Karlsruhe

KERNFORSCHUNGSZENTRUM KARLSRUHE

Institut für Neutronenphysik und Reaktortechnik

Projekt Schneller Brüter

KfK 2546

# Further Development of the LMFBR Accident Analysis Codes HOPE and KADIS: Automatic Data Transfer, New Equation of State

E.A. Fischer, G. Arnecke

Kernforschungszentrum Karlsruhe GmbH., Karlsruhe

Abstract

To provide suitable tools for the analysis of hypothetical unprotected transient overpower accidents in liquid metal cooled fast breeder reactors, the codes HOPE and KADIS were further developed. HOPE analyses the initiating phase of a reactivity ramp accident in an irradiated core, KADIS is a core disassembly code. Besides some minor improvements in HOPE, an automatic data transfer from HOPE to KADIS was organized. In addition, a new equation of state, which includes fission gas pressures, was developed and introduced in KADIS. The system of the two codes allows a consistent treatment of fission gas effects in both the initiating and the disassembly phase. Furthermore, care was taken to make sure that the fuel-coolant interaction models in both codes are as well compatible as feasible.

A reference transient overpower accident, initiated by a 15 ¢/sec reactivity ramp, was analyzed, using a melt fraction criterion for pin failure.

To make sure that an energetic core disassembly occurs, the rather pessimistic assumption of mid-plane pin failure was made, though a failure in the upper part of the pin is considered to be much more likely, which is also supported by experiments. In this accident, the fission-gas driven fuel ejection through the rip causes a positive fuel motion reactivity. On the other hand, fission-gas pressure disperses fuel during the super-prompt critical disassembly phase, and the total energy release is still less than predicted in an earlier analysis of the same accident sequence with the codes CAPRI-2 and KADIS.

In addition, the 15 ¢/sec ramp accident was also analyzed with the more mechanistic burst stress failure criterion, but still sticking to the pessimistic assumption of mid-plane failure. In this case, the predicted energy release is again considerably less.

# Weiterentwicklung der Programme HOPE und KADIS für die Analyse von Störfällen in schnellen Brutreaktoren: Automatische Datenübertragung, neue Zustandsgleichung

## Zusammenfassung

Um geeignete Codes für die Analyse von hypothetischen Leistungsstörfällen in natriumgekühlten schnellen Brutreaktoren bereitzustellen, wurden die Codes HOPE und KADIS weiterentwickelt. HOPE analysiert die Einleitungsphase eines Reaktivitätsrampen-Störfalls in einem abgebrannten Core, KADIS ist ein Code zur Analyse der Disassembly-Phase eines Störfalls. Außer einigen kleinen Verbesserungen in HOPE wurde eine automatische Datenübertragung von HOPE nach KADIS organisiert. Eine neue Zustandsgleichung, die auch Spaltgaseffekte beschreibt, wurde entwickelt und in KADIS eingebaut. Das so gekoppelte Code-System erlaubt eine konsistente Behandlung von Spaltgaseffekten in der Einleitungs- und Disassembly-Phase.

Ein Referenzleistungsstörfall, der durch eine Reaktivitätsrampe von 15 ¢/sec eingeleitet wird, wurde analysiert unter Annahme eines Schmelzfraktionskriteriums für das Stabversagen.

Um sicherzustellen, daß der Störfall in eine energetische Kernzerlegungsphase einläuft, wurde die pessimistische Annahme gemacht, daß der Stab in der Mittelebene versagt, obwohl ein Versagen im oberen Teil viel wahrscheinlicher ist, wie auch durch Experimente bestätigt wird. Bei diesem Störfall führt das Brennstoffausspritzen durch den Spaltgasdruck zu einer Reaktivitätszufuhr. Andererseits wirkt der Spaltgasdruck in der überprompt kritischen Kernzerlegungsphase als Abschaltmechanismus, und die gesamte Energiefreisetzung liegt deutlich niedriger als die, die in einer früheren Analyse desselben Störfalles mit den Programmen CAPRI-2 und KADIS vorhergesagt wurde.

Außerdem wurde der Reaktivitätsstörfall mit 15 ¢/sec auch noch analysiert unter Annahme des mechanischen Berstdruck-Versagenskriteriums, wobei aber immer noch Versagen in der Mittelebene postuliert wurde. Die Energiefreisetzung ist in diesem Fall nochmals wesentlich niedriger.

## 1. INTRODUCTION

It has been emphasized recently in the literature that hypothetical core disruptive accidents in an irradiated LMFBR core will be greatly mitigated by the presence of fission products, especially of fission gases. A first attempt [1] to account for fission product effects in the disassembly phase of an unprotected transient overpower (TOP) accident has shown the potential of the gas pressure as a shutdown mechanism. However, the initial conditions for the disassembly calculation were determined in a rather crude way, and it was not attempted to include fission gas effects also in the predisassembly calculation.

It is, therefore, desirable to perform a more consistent analysis of the whole accident sequence, where the fission gas effects are modeled both in the predisassembly and disassembly phase.

The tools presently available at Karlsruhe for the simulation of the predisassembly phase of hypothetical core disruptive accidents are the codes CAPRI-2 and HOPE. CAPRI-2 can treat both unprotected transient overpower and loss of flow accidents [2]. It was used, in connection with the disassembly code KADIS [3], for a rather detailed analysis of hypothetical core disruptive accident for the SNR-300. This work was greatly facilitated by an automatic transfer of data from the predisassembly to the disassembly code. The analysis for the SNR-300 puts the main emphasis on accidents in the fresh core. It was realized that the modeling for the irradiated core is not as detailed as for the fresh core. Especially, the TOP analysis did not include fission gas effects. It is, therefore, to be expected that the calculated energy release data are too conservative.

The code HOPE, which was developed at UCLA [4], can treat only TOP accidents, and was designed especially for the analysis of accidents in irradiated cores. Thus, the modeling is, in some areas, more detailed than in CAPRI-2; it includes effects like gas release, pressurization of the fuel pin cavity, expulsion of fuel and gas after pin failure. Thus, it was decided to use HOPE and KADIS for a TOP analysis which includes fission gas effects in a consistent way.

---

Zum Druck eingereicht am 21.3.1978

To reach this goal, some further development of both codes was necessary which includes organising an automatic data transfer from HOPE to KADIS and the development of a new equation of state in KADIS. In addition to work towards this main goal, a new equation of state for $UO_2$, based on a recent data evaluation, was introduced in KADIS. Case studies were carried out for the end-of-life core of the SNR-300.

## 2. IMPROVEMENTS IN HOPE

### 2.1 Comments on the Code HOPE

HOPE is an integrated program for simulating the predisassembly part of an unprotected LMFBR whole core accident, initiated by a reactivity ramp. The code was developed at UCLA [4]. In brief, the phenomena treated by HOPE are the following:

1) Point neutron kinetics
2) Steady-state fuel behavior, including heat transfer, density changes due to restructuring, and fission gas release
3) Transient heat transfer
4) Fuel melting and formation of a molten fuel-fission gas cavity
5) Stress and strain analysis of fuel and clad, pin failure
6) Fuel and fission gas ejection
7) Fuel fragmentation and fuel-coolant interaction
8) Fuel movement and reactivity feedback

A detailed description of the physical models is available in the literature [4], and will not be repeated here. Comments for the use of the code are given in Section 2.3. The input description of the Karlsruhe version, and a sample problem are given in the Appendix.

Some minor modifications which were made on the code concern the following points:

a) In a mild FCI, the pressure in the FCI zone is relieved through expansion of the zone in upward and downward direction. In case the pressure drops below the inlet pressure, re-entry of the lower slug should occur. The equations were slightly modified compared to the HOPE version documented in [4] so that re-entry of the lower slug can be described.

b) Some material properties were changed, the most important one being the thermal conductivity of the fuel. The new values were taken from Schmidt [5] for solid fuel, and assumed constant at 0.022 W/cm K for liquid fuel.

## 2.2 Fission Gas Behavior Model in HOPE

The steady-state release of fission gas from the fuel is calculated in HOPE from the empirical relationship by Dutt [6], which postulates 100% release in restructured fuel, whereas the release in unrestructed fuel is described by an analytic expression. The predictions of the Dutt relation were extensively compared to a fission gas behavior model, and found to be well compatible with it [7,8].

The gas behavior during the transient is modeled as follows. A specified fraction of the gas retained in the fuel, typically 20%, is considered to reside on grain boundaries, and is released as the fuel reaches the melting isotherm. The rest is released in proportion to the melt fraction. The released gas is assumed to be in temperature equilibrium in the central cavity.

In reality, the transient fission gas behavior is more complicated and may be classified from its physical effects into two characteristic phases. The first phase is the fast precipitation of gas bubbles in the unrestructured fuel, which leads to transient fuel swelling. No attempt was made to account for this effect in HOPE, because the code does not allow for further swelling once the fuel starts to melt. In

the second phase, gas bubble migration in the thermal gradient leads to substantial gas release even before the fuel reaches the melting isotherm in a slow transient. However, in a rapid transient, bubble migration is too slow compared to the heating rate, and significant release occurs only when the fuel melts.

The behavior in the second phase can be approximately simulated in HOPE without changing the original model. Thus, the early release in a slow transient can be simulated by assuming 100% gas release, as the fuel reaches the solidus. The influence of this early release was studied by investigating two cases, one with 20% and one with 100% release at the solidus.

## 2.3 Fuel-Coolant Interaction Model

The molten fuel-coolant interaction (FCI) plays an important role in a TOP accident. Therefore, the models used to describe this interaction in HOPE and in KADIS will be briefly outlined here. In principle, both treatments should be consistent, because they are based on the model by Cho, Ivins, and Wright; however, there are certain characteristic differences, due to the basically different description of the reactor core in HOPE and in KADIS, which will also be briefly discussed.

In HOPE, the fuel fragmentation process, which occurs after the ejection of a molten fuel-fission gas mixture into the coolant channel, is modeled parametrically. It is assumed that fragmentation occurs in a number of steps. At each step, a particle is split into new ones, each with half the initial volume. Both the number of steps (typically 4), and the total fragmentation time, are input parameters. Fragmentation is cut off if the subcooling of the bulk sodium becomes less than a few degrees and if the void fraction exceeds a certain limit (fission gas cutoff).

The interaction zone in the coolant channel, which can expand axially, is assumed to have uniform temperature, pressure, and density. Heat transfer from the fuel particles to the coolant is described by the quasi-steady-state heat transfer model by Cho and Wright [4]. The state of the interaction zone is determined by three differential equations: coolant energy conservation, equation of state of the coolant, and an equation of constraint on the interaction zone. A more detailed description was given by Rumble [4].

In principle, the FCI model in KADIS [3] includes the same features. For a consistent treatment, the important FCI parameters, like FCI time in each channel, are transferred from HOPE to KADIS (see Section 3). However, there are some characteristic differences in the modeling used in the two codes: The fuel fragmentation is described in KADIS by a single time constant. Heat transfer is modeled as in HOPE; however, it is calculated only if the fuel temperature exceeds a threshold value, and is cut off if a certain void fraction is exceeded. Furthermore, the state of FCI region is determined in KADIS node by node. Thus, only two differential equations are necessary, namely for coolant energy conservation, and the equation of state of the coolant. This description is more detailed, because the assumption of a uniform interaction zone is relaxed. However, mass exchange between nodes is not possible; thus, expanding sodium vapor moves all the fuel in the node, not only the ejected fuel.

Most of these points in which the FCI model in KADIS differs from the original Cho-Wright concept are inevitable , if FCI is to be included in a Lagrangian hydrodynamic model of the reactor core. Therefore, the differences are acceptable in all the cases where a hydrodynamic core disassembly model is appropriate.

## 2.4 Comments on the Use of the Code HOPE

The version of HOPE used for this work is limited to 13 channels, 20 axial nodes in each channel, and 10 radial fuel nodes in the pin. In addition, a 30 channel version is available at Karlsruhe.

For a run without use of external units, the core space required is 480 K bytes. If external units are used, space required for the buffer has to be added to the core space.

The code has the following output capabilities, for which external units must be specified:

Plot data can be written on external units. The code writes the array VPL10 (124 rows) on unit 10, and VPL11 (190 rows) on unit 11. The variables contained in these two arrays, and their physical meaning are explained in Appendix D. The plots displayed in this paper (Fig.6 to 9) were obtained with the routine PLOTCP described by Zimmerer [9].

The transfer data for a disassembly calculation can be stored on unit 20. In this case, it is also necessary to write the reactivity table on unit 21.

In addition, the code has the capability to write the power history on an external unit (unit 9), for use in a later run. In this later run, the power history is then read in, and the neutron kinetics equations in the code are not used. This option is also of interest for the analysis of in-pile transient experiments, for which the power history is specified independently. More specifically, the code writes the variables TIME (accident time), TR2 (main time step), and PJ1 (normalized power).

An example for the job control cards is given in Appendix C. Note that a DD statement should be replaced by Dummy if an external unit is not used.

The structure of the code with its different subroutines, as shown in Fig.4, will be briefly explained.

MAIN — The MAIN program reads the input data, solves the neutron kinetics equations. It calls the thermohydraulics moduls STEMP (at time zero) and TEMP (after each main time step). It also calls the output routine INFO

STEMP — calculates the steady state heat transfer, fission gas retention, and fuel restructuring

TEMP — calculates the transient heat transfer, fission gas release and cavity properties

COOL — calculates the transient coolant properties, and the reactivity feedback

MOVE — determines the time and location of pin failure, and calculates the fuel ejection

CIWM — contains the fragmentation and fuel-coolant interaction models

FAMM — calculates the velocity and position of the ejected fuel particles

INFO organizes the printout and most of the writing of data on external units.

Note that HOPE does not have an automatic time step control. The initial main time step may be fairly large, in a typical case 0.05 sec, whereas the fuel-coolant interaction calculation requires a much smaller time step, typically $\leq 5\times10^{-4}$ sec. One must, therefore, make sure to select the criteria for the time step switch such that the switch occurs before the first pin failure.

## 3. DATA TRANSFER HOPE-KADIS

### 3.1 General Remarks

Whereas the thermal and hydraulic conditions in HOPE are described in the fuel pin - coolant channel geometry, KADIS is a hydrodynamics code where the composition in a core mesh cell is essentially assumed to be homogeneous. Therefore, the data set to be transferred from HOPE to KADIS has to consist of average values over a core mesh cell, which are essentially the volume fractions, temperatures, and densities of the core components fuel, sodium, stainless steel, and fission gas.

Also included in the transfer data set are the Doppler coefficients which are interpolated from wet and dry conditions with the actual void fractions and which reflect the actual core voiding patterns at switch over. If the fuel has not reached the liquidus, the mass of gas still retained in the fuel is also transferred. In addition, some important FCI parameters for each of the failed channels are included.

The switch over point to disassembly is usually defined when the enthalpy averaged temperature over the hottest fuel pellet reaches about 3100 to 3200°C. Case studies show that at this point, the gas pressure in the cavities is of the order of several hundred bars, and is rapidly

increasing, inspite of the ejection process, which is still going on. Thus, the rupture stress of the clad is exceeded, and the clad breaches over a large portion of the core within a few milliseconds, resulting in very little axial fuel motion within the pin. At the same time, relative motion of the other core materials, like sodium expulsion, is going on at a moderate rate. Switch over to disassembly is usually predicted when the core has reached a prompt critical state and the power level is high. This leads to a fast heating rate of the fuel, and it is reasonable to assume that at this point, the high pressure cavity gas fills the available void space in the associated core volume, unhindered by the presence of the clad. This space includes any void space in the coolant channel, and the space associated with the porosity of the fuel. Thus, the gas pressure acts on the neighboring regions of the core both in axial and radial direction, and through its high compression can lead to core disassembly.

Under these conditions, the homogeneous model used in a disassembly code is generally valid, and it is justified to continue the analysis with the KADIS code.

## 3.2 Definition and Calculation of the Transfer Data in HOPE

The preparation of the transfer data in HOPE requires some care, because an attempt is made to bridge the two different models in HOPE and in KADIS; in such a way one is as close to a consistent treatment as possible. However, due to the differences in models, compromises are necessary, and it may be of interest to explain them here in some details.

Those quantities which must be defined carefully are the temperatures, volume fractions, and densities of the core components fuel, sodium, SS, and fission gas. On the other hand, the definition of the reactivity coefficients is straight forward and needs no further discussion.

a) Temperatures of the Core Components

The pellet averaged fuel temperature is defined as the enthalpy-average over the different radial nodes of the pellet. This averaging (including the heat of fusion) is carried out in the modul TEMP. Analogous to the treatment in KADIS, it is assumed that the temperature increases from $T_m$ to $T_m+1$ as the melt fraction goes from 0 to 1. The temperatures of the other core materials are defined in a straight forward manner; however, note that the SS temperature is an average between clad and structural material.

b) Geometric Volume Fractions

The geometric volume fractions in the unit cell are defined as follows

$$V_{cell} = V_{pin} + V_{Na} + V_{str} \quad (\text{at } t=0)$$

$$v_f = \pi (R_{NT}^2 - R_l^2)/V_{cell}$$

$$v_{gas} = \frac{\pi R_{melt}^2}{V_{cell}} \frac{V_{cav}^{gas}}{V_{cav}}$$

$$v_{Na} = \frac{V_{cell} - V_{pin} - V_{str}}{V_{cell}}$$

$$v_{SS} = \frac{V_{clad} + V_{str}}{V_{cell}}$$

The geometric volume fractions are retained for fuel, SS, and gas; however, the sodium volume fraction will be redefined below and is subject to the condition

$$v_{Na} \leq 1 - v_f - v_{ss} - v_{gas}.$$

c) Densities

To make sure that the fuel mass, temperature, and density are consistent, the fuel mass in an axial node is renormalized at the last time step of the HOPE run using the equation

$$m_f = \sum_{\text{Rad.Nodes}} V_{\text{node}} \, \rho_{th} \, (T_f) \left[1-\text{Por(Node)}\right]$$

where the porosity Por is defined for each restructuring zone, and zero if the node has reached or exceeded the melting temperature. The redefind mass may be as much as 1-2% lower than the original mass, due to the fact that the density at high temperatures is lower, but HOPE does not explicitly account for the axial fuel expansion.

The fuel density is then defined by

$$\rho_f = \frac{m_f}{v_f \cdot V_{\text{cell}}}$$

The sodium density is defined as the liquid density at the sodium temperature

$$\rho_{Na} = \rho_{liq} \, (T_{Na})$$

This requires a new definition of the sodium volume

$$v_{Na} = \frac{m_{Na}}{\rho_{Na} \, V_{\text{cell}}}$$

which is, however, subject to the above condition. Thus, in case of partial or complete voiding, the sodium mass is concentrated in a small volume at liquid density, thus leading to a high void fraction.

This concept seems to be compatible with the KADIS model.

Finally, the gas density is given by

$$\rho_{gas} = \frac{m_{cav}^{gas}}{V_{cav}^{gas}}$$

and the density is defined in a straight forward manner.

d) Gas Retained in the Fuel

The fission gas mass retained in the fuel is normalized to one gram of solid fuel in the node

$$GSC = \frac{m_{gas}}{m_{fsol}}$$

$$\text{where } m_{fsol} = \begin{cases} m_f & \bar{T}_f < T_m \\ m_f\,(T_m + 1 - \bar{T}_f) & T_m < \bar{T}_f < T_m + 1 \end{cases}$$

If $\bar{T}_f \geq T_m + 1$, GSC is set equal to zero, and the gas still contained in the outer fuel nodes is considered to be released.

## 3.3 Description of the Data Management

The organisation of the data transfer from HOPE to KADIS at the switch over point will be briefly described in this section. The schematics of the data flow is presented in Fig.4.

At the switchover time, the transfer data are calculated in different subroutines of HOPE, and the subroutine INFO writes them on an external unit. In addition, the HOPE run continues for a few time steps beyond the switchover point, in order to extrapolate the reactivity due to sodium voiding and fuel motion into the disassembly phase. The history of the net and the Doppler reactivity ("reactivity table") is then stored on an external unit, for use in the KADIS input.

In the next step, the modul KAINPT of the predisassembly code CAPRI-2 [2] is used to read the transfer data, and to convert them to the units and to the format required for the KADIS input file. This procedure makes it necessary to perform a CAPRI-2 run, which is, however, a dummy run in the sense that the thermohydraulic modules of the code are not used. The data from KAINPT are then combined with the reactivity worth curves to produce the KADIS input file. In the last step, the simulation of the disassembly phase with KADIS can be performed.

In the HOPE studies carried out so far for the SNR-300, the input data concerning the core and the channel geometry, and the reactivity worth curves, were prepared by the modul READIN of CAPRI-2 (Fig.4). With this procedure, it is made sure that the input data for HOPE are consistent with those used for the earlier simulation with CAPRI-2, which were reported by Fröhlich et al. [10].

## 4. New Equation of State in KADIS

### 4.1 General Remarks

In the disassembly code KADIS, the equation of state (EOS) serves to calculate the pressure as a driving force for core disassembly. The pressure is obtained from the internal energy of the fuel, produced by fission heating, and from the available volume for a mesh cell. Thus, the EOS provides the link between the neutronic and hydrodynamic calculation.

For most of the earlier KADIS calculations [3] the so-called ANL equation of state was used, which was essentially obtained by Menzies in 1966, using the principle of corresponding states. In the frame of the present work, the treatment was updated by implementing a completely new equation-of-state routine in KADIS. This new routine covers both the cases where fission gas is absent, or present in the mesh cell. In the case without fission gas, the equation of state SSTEOS is used, which is based on a recent evaluation of thermodynamic data for $UO_2$ [11]. In the other case, which is the more important one for accidents in an irradiated core, the equation FIGASEOS provides an adequate treatment of pressure build-up in the presence of fission gas, which is reasonably consistent with the treatment in HOPE. Both cases will be described in the following sections.

### 4.2 The Equation of State SSTEOS

The equation of state SSTEOS for $UO_2$ is based on a recently published data evaluation [11], where the Significant Structure Theory (SST) by Eyring was employed to extrapolate the data to the critical point. This evaluation is consistent with most of the available experimental thermodynamic data, including the liquid density [12], the enthalpy in the solid and in the liquid state [13], and the recent vapor pressure measurements over liquid $UO_2$ [14,15] Therefore, this equation of state can be considered as fairly up-to-date, although the assumption is still made that $UO_2$ data are representative also for fast breeder fuel $(U, Pu)O_2$. However, the routine has an option which allows to specify the melting point, and the liquid density at the melting point, so that the values for mixed oxide can be used.

SSTEOS for liquid $UO_2$

In the liquid range, analytical fits to the published equation-of-state data were constructed. In the absence of non condensable gases, one has to consider both single-phase and two-phase conditions. The fits use the internal energy U and the reduced density $\rho_r = \rho/\rho_c$ as independent variables. The equations are valid between the melting point and the critical point, defined by $T_c$ = 7560K, $p_c$ = 1220 bar, $\rho_c$ = 1.66 g/cm$^3$; both points are well approximated.

The procedure to calculate the pressure and the temperature of the fuel is the following: First, calculate the saturation temperature corresponding to the density $\rho_r$ and to the internal energy U:

$$T_S(\rho_r) = \begin{cases} 3120 + 1463.4(5.27-\rho_r) - 89.14(5.27-\rho_r)^2 & \text{for } \rho_r > 2.747 \quad (1) \\ 7550 - 805.6(\rho_r-1)^2 + 216.44(\rho_r-1)^3 & \text{for } \rho_r < 2.747 \quad (2) \end{cases}$$

and

$$T_S(U) = 3120 + 1.8687\ (U-U_1) - 4.0720^{-5}\ (U-U_1)^2 \qquad (3)$$

where U is in J/g, and $U_1$ is the energy of liquid $UO_2$ at the melting point.

Obviously, if $T_S(\rho_r) > T_S(U)$, the volume required for the fuel to be in the two-phase domain is available. Therefore, the temperature is $T_S(U)$ and the pressure is the saturation pressure

$$T = T_S(U) \qquad (4)$$

$$\log p(\text{bar}) = 31.668 - 35073/T - 2.6812 \ln T \qquad (5)$$

In the case of single-phase pressures, $T_S(\rho_r) < T_S(U)$, the calculation is somewhat more compliceted. One finds $U_{sat}$ and $p_{sat}$, the values on the saturation line corresponding to $\rho_r$:

$$T_{sat} = T_S(\rho_r) \tag{6}$$

$$U_{sat} = U_1 + 2.2945 \times 10^4 \{1 - [1 - 0.4664 \times 10^{-4}(T_{sat} - 3120)]^{1/2}\} \tag{7}$$

$$\log p_{sat} = 31.668 - 35073/T_{sat} - 2.6812 \ln T_{sat} \tag{8}$$

Note that eq. (7) is the inversion of eq. (3). Furthermore, one obtains the temperature and pressure

$$T = T_{sat} + (U - U_{sat})/C_v(\rho_r) \tag{9}$$

$$p = p_{sat} + \frac{\partial p}{\partial T}(\rho_r)\ (T - T_{sat}) \tag{10}$$

It is assumed that $C_v$ and $\partial p/\partial T$ for liquid $UO_2$ can be approximated by the values on the saturation line, which were produced by the SST, and are given as functions of $\rho_r$

a) $\rho_r > 2.747$

$$C_v = 0.27364 - 8.6915 \times 10^{-3}(5.27 - \rho_r) - 2.8806 \times 10^{-4}(5.27 - \rho_r)^2 \tag{11}$$

$$\frac{\partial p}{\partial T} = 56.8 - 39.66(5.27 - \rho_r) + 7.823(5.27 - \rho_r)^2 \tag{12}$$

b) $\rho_r < 2.747$

$$C_v = 0.23256 + 6.4388 \times 10^{-3}(\rho_r - 1) + 1.6093 \times 10^{-3}(\rho_r - 1)^2 \tag{13}$$

$$\frac{\partial p}{\partial T} = 0.980 + 2.349(\rho_r - 1)^2 - 0.2412(\rho_r - 1)^3 \tag{14}$$

The relationship defined by equations (1) through (14) are shown in Fig. 1-3. Fig. 1 gives the density of the liquid, and the saturated vapor. It is easily seen that the law of rectilinear diameter holds for these curves. Fig. 2 and 3 show the temperature and the pressure vs. internal energy. In the single-phase domain, for a given $V_r$ (or $\rho_r$), they are approximated by straight lines.

In deriving the above equations, the following values for the melting point, the liquid density at the melting point, and the heat of fusion were assumed

$$T_m = 3120 \text{ K}$$

$$\rho_\ell(T_m+1) = 8.75 \text{ g/cm}^3$$

$$H_f = 274.4 \text{ J/g}$$

In addition, it was assumed that the temperature rises by 1 K during melting. The associated change in enthalpy is neglected in view of the uncertainties in $H_f$. The option to specify $T_m$, $\rho_\ell$, and $H_f$ is discussed below.

SSTEOS for solid and partially molten $UO_2$

If $UO_2$ is solid, or only partially molten in an outer cell of the core, it usually does not develop a high pressure on its own, but it may be compressed by material accelerated by high driving pressure in an inner cell. Therefore, pressure build-up must be allowed for, but it may be estimated in a fairly crude manner.

As to the calculation of the temperature, one has to make sure that the energy scale is consistent with the one used in the predisassembly analysis, i.e. in HOPE. Therefore, if $U < U_m$ (melting energy), the temperature is obtained by inverting the U(T) relation suggested by Gibby et al. [16], which is used in HOPE. If $U_m = 1116.4$ J/g is exceeded, the melt fraction is

$$X = (U-U_m)/H_f$$

and

$$T = T_m + X$$

Then, the saturation pressure is obtained from eq. (5). It is always small. However, if the fuel is to be compressed beyond its theoretical density, the pressure is calculated from

$$p = \frac{1}{\beta_t} \frac{\rho-\rho_{th}}{\rho} \qquad (15)$$

where both the isothermal compressibility $\beta_t$ ($=0.62\times10^{-12}$ $cm^2/dyn$ for solid $UO_2$) and the theoretical density $\rho_{th}$ are interpolated between solid and liquid in the case of partially molten fuel. The solid density $\rho_{th}$ is taken from Christensen [12].

Option to specify $T_m$, $\rho_\ell$, and $H_f$

The routine allows the user to specify $T_m$, $\rho_\ell$, and $H_f$; thus it is possible to use, for example, the values preferred for $(U,Pu)O_2$.

If an input value for $T_m$ is used, it is assumed that the U versus T relation (3) is not affected. However, the density $\rho_\ell = 8.75$ $g/cm^3$ is now assigned to the liquid at the melting point $T_m$, and the saturation temperature $\tilde{T}_S(\rho_r)$ as a function of the density is redefined by the equation

$$\tilde{T}_S(\rho_r) = T_m + [T_S(\rho_r) - 3120] \frac{7550-T_m}{4430}$$

where $T_S(\rho_r)$ is given by eqs. (1) and (2).

If the liquid density $\rho_\ell$ at the melting point is specified, the fuel density over the whole range up to the critical point is modified by the same factor. This is simply done by defining

$$\rho_c = 1.66 \frac{\rho_\ell}{8.75}$$

A specification of $H_f$ has only the effect of shifting the energy $U_1$ at the melting point.

Additional Comments

Once the pressure has been found for the estimated volume available for the fuel, one has to account for the compression of the sodium and steel, which may lead to a larger volume for the fuel, and to a reduced pressure. The final pressure is found by an iteration procedure in much the same way as described for the VENUS code [17].

Heat transfer from molten, fragmented fuel to sodium, and the vapor pressure of sodium can be included above a certain threshold temperature, according to a model described by Schmuck [3].

The speed of sound in liquid $UO_2$ is estimated in the same way as in the VENUS code [17]. For convenience, the equations are listed in the Appendix.

## 4.3 Equation of State FIGASEOS

FIGASEOS calculates the pressure in a mesh cell in the presence of non-condensable gases. The model can be described as follows:

a) The fuel vapor pressure, calculated from eq. (5) in Section 3.2, contributes to the total pressure. However, no single phase liquid pressures are allowed, because the fuel is much less compressible than gas, or even sodium.

b) The gas mass in a particular mesh cell may increase during a time step due to release of additional gas, if the fuel has not reached the liquidus, and still contains retained fission gas. As present, there is no conclusive information on the magnitude of the time delay for gas release from molten fuel. Therefore, the time delay was modeled parametrically with a time constant, which is an input parameter. The equation is

$$\dot{m}_g = \frac{1}{\tau_r} (m_{go} - m_g)$$

where $m_g$ and $m_{go}$ is the mass of gas released with and without time delay. As there is indication from experiments in the VIPER reactor [18] that the time delay, if any, is small, the reference case was run without time delay.

c) Heat transfer from the fuel to the gas is modeled, using a time constant which is an input parameter. Thus, any case between zero heat transfer, and the gas in thermal equilibriums with the fuel, can be treated.

d) Given the gas mass and temperature, according to b) and c), and the new volume of the mesh cell, it is assumed that the gas expands (or is compressed) adiabatically into the now available volume. In cells with liquid sodium, gas volume fractions are low, typically of the order of 1 %. One can easily convince himself that the compressibility of sodium must be accounted for in such a case. Assume, for example, that the gas is under a pressure of 1000 bar. Then, the sodium ($\sim$ 50 v/o) is compressed by 2 - 3 %, which more than doubles the available gas volume. Therefore, the pressure is obtained by solving the volume balance equation in a cell

$$V_{Na}(p) + V_{ss}(p) + V_g(p) + V_f = \text{Volume} \qquad (16)$$

The procedure is described below.

e) The vapor pressure of sodium is neglected. However, heat transfer from molten, fragmented fuel can be included. As a consequence, the sodium expands, and reduces the space available for the gas, thus leading indirectly to an increase of the gas pressure.

The procedure to solve the above volume balance equation (16) will now be described. The density-pressure relationship is assumed to be given by the Murnaghan equation

$$\rho = \rho^o\left(1+ \frac{\beta_{el}}{\beta_{eo}} P\right)^{1/\beta_{el}} \qquad (17)$$

for sodium, and for steel. (The compressibility of steel is small and could have been neglected.) For the gas, the adiabatic equation

$$P_g V_g^{\gamma} = P_g^o (V_g^o)^{\gamma} \qquad (18)$$

holds, and P is the sum of gas and fuel vapor pressure.

The set of equations (16-18) is solved by iteration, using the variable $x = P_g^{-1/\gamma}$. Then, from equation (18), $V_g$ is given by

$$V_g = \left(\frac{RT_o m}{AV_{go}}\right)^{1/\gamma} \cdot V_{go} \cdot x \tag{19}$$

Assume that an initial value $\tilde{x}$ for x is given. Then, a step of the iterative procedure is carried out as follows: $V_{Na}$ and $V_{SS}$ are approximated as a linear functions of $x-\tilde{x}$;

$$V_{Na}(x) \approx V_{Na}(\tilde{x}) + \frac{\partial V_{Na}}{\partial x}(x-\tilde{x}) \tag{20}$$

where the derivative is obtained from equation (17)

$$\left.\frac{\partial N_{Na}}{\partial x}\right|_{\tilde{x}} = \frac{V_{Na}(\tilde{x})\cdot\gamma}{\tilde{x}^{1+\gamma}(\beta_{eo}+\beta_{e1}\tilde{P}_g)}$$

Then, the linearized equation (16) for x can be easily solved, and $P_g$, $V_{Na}$, $V_{SS}$ are obtained. If necessary, the procedure is repeated.

It was found that this method converges in most cases after one or two iterations.

## 5. Analysis of Transient Overpower Accidents with the System HOPE-KADIS

Unprotected transient overpower (TOP) accidents were analyzed for the end of life (EOL) configuration of the SNR-300, Mark 1A core. A detailed description of this core configuration was given elsewhere [10]. However, some features which are important for an understanding of the results will be briefly summarized.

The reactor has a thermal power of 754 MW. The EOL configuration corresponds to 441 days of operation, with a peak burn up of 76000 MW /to. Both the radial and axial power distribution are rather flat. The maximum linear heat rate is about 290 W/cm in the central channel, and 230 W/cm in the channel with the lowest power.

For the analysis, the reactor is divided into 13 radial channels. Nine channels represent the inner zone of the core, channels 10 and 11 are used for the outer core zone, with a higher Pu enrichment. The last two channels represent the radial blanket. In the axial direction, the model includes the core, which is divided into 13 nodes, and both the lower and upper axial blanket with 3 and 4 nodes. The configuration is shown in Fig. 5 Note that the model for the simulation takes account of the axial nodes 7 to 26 in Fig. 5.

### 5.1 Simulation of a 15 ¢/sec Ramp Accident using the Melt Fraction Criterion

The TOP accident initiated by a 15 ¢/sec reactivity ramp was analyzed earlier with the CAPRI-KADIS system [10], using a melt fraction criterion to define pin failure in a channel. However, this analysis did not account for fission gas effects in a consistent way, and it is, therefore, of great interest to repeat the same case with the HOPE-KADIS system.

Most of the parameters are the same as used for the CAPRI-KADIS simulation [10] .The data which are different are shown in Table 1. The failure melt fraction of 50 %, as used in [10], is probably too large, because both experimental results from TREAT, and a detailed analysis of the fuel pin behavior indicate that failure may occur earlier. Therefore, a 30 % melt

Table 1: Parameters used for the Analysis of a 15 ¢/sec Reactivity Accident, with a melt fraction failure criterion

HOPE Parameters

| | |
|---|---|
| Pin failure melt fraction | 30 % |
| Cut length | 5 cm |
| Fragmentation time | 10 msec |
| Particle Radius | 117 μ |
| Temperature at switchover to disassembly | 3150°C |

KADIS Parameters

| | |
|---|---|
| Threshold temperature for heat transfer to sodium | 2705°C |
| Mixing time constant | 10 msec |
| Particle radius | 117 μ |
| Time constant for heat transfer fuel-gas | 0.02 sec |

Table 2: Results for a 15 ¢/sec TOP using a thermal failure criterion

| | Fresh Core | EOL Core | |
|---|---|---|---|
| | CAPRI/KADIS | CAPRI/KADIS | HOPE/KADIS |
| Pin Failure | | | |
| Assumed Failure melt fraction | 60 % | 50 % | 30 % |
| Time of first failure (sec) | 6.7 | 8.72 | 8.73 |
| Normalized Power at first failure | 5.3 | 4.2 | 4.2 |
| Net Reactivity ($) | 0.50 | 0.41 | 0.41 |
| Failure Sequence, channels | 1,2,3,10,4 | 1,2,10,3,4,5,6,7,8,9,11 | |
| FCI Data, Channel 1 | | | |
| Mass ratio fuel/sodium | 6.0 | 4.9 | 3.4 |
| axial height of failure position | 50 % | 53 % | 47 % |
| Data at Switchover to Disassembly | | | |
| FCI time in channel 1 (msec) | 83 | 35 | 86 |
| Normalized Power | 399 | 1251 | 2029 |
| Net reactivity/ramp ($; $/sec) | 1.081/15.3 | 1.108/15.9 | 1.146/-28 |
| Doppler reactivity/ramp ($;$/sec) | -.727/-25.1 | -1.175/-80.6 | -1.251/-124 |
| Void reactivity/ramp ($;$/sec) | .759/40.3 | .970/96.3 | .791/71 |
| Fuel reactivity/ramp ($;$/sec) | - | - | .283/25 |
| Disassembly Data | | | |
| Duration of core disassembly (msec) | 2.67 | 2.30 | 1.42 |
| Energy in the molten fuel (MWsec) | 1182 | 2940 | 1952 |
| Mass of molten fuel (%) | 57 | 88 | 76 |
| Average temperature of molten fuel (°C) | 2889 | 3186 | 3075 |

Table 3: Fission Gas Pressure (in Bar) at the Begin of the Disassembly Phase

(Case with Melt Fraction Criterion)

| Axial Core Node | Inner Core Region | | | | | | | | | Outer Core Region | |
|---|---|---|---|---|---|---|---|---|---|---|---|
| 16 | 1 | 1 | 1 | 1 | 5 | 1 | 1 | 1 | 1 | 1 | 1 |
| 15 | 1 | 1 | 12 | 13 | 111 | 12 | 4 | 2 | 1 | 1 | 1 |
| 14 | 3 | 2 | 70 | 58 | 255 | 50 | 31 | 43 | 16 | 3 | 14 |
| 13 | 4 | 4 | 3 | 89 | 296 | 79 | 60 | 15 | 32 | 4 | 30 |
| 12 | 13 | 12 | 20 | 117 | 398 | 180 | 138 | 25 | 73 | 12 | 53 |
| 11 | 14 | 13 | 22 | 12 | 115 | 15 | 14 | 14 | 9 | 13 | 8 |
| 10 | 15 | 13 | 23 | 25 | 213 | 24 | 23 | 19 | 12 | 13 | 11 |
| 9 | 15 | 13 | 215 | 344 | 668 | 309 | 316 | 68 | 207 | 13 | 36 |
| 8 | 14 | 13 | 494 | 334 | 647 | 318 | 324 | 67 | 159 | 365 | 75 |
| 7 | 13 | 12 | 444 | 181 | 433 | 157 | 147 | 20 | 74 | 333 | 36 |
| 6 | 4 | 4 | 209 | 90 | 331 | 69 | 61 | 14 | 29 | 142 | 27 |
| 5 | 2 | 2 | 73 | 39 | 197 | 27 | 18 | 4 | 7 | 48 | 2 |
| 4 | 1 | 1 | 14 | 3 | 19 | 1 | 1 | 1 | 1 | 4 | 1 |
| | 1 | 2 | 3 | 4 | 5 | 6 | 7 | 8 | 9 | 10 | 11 |

limit of the voided zone

Radial Channel Number

Table 4: Influence of a time delay for fission gas release in the disassembly calculation (Reference accident)

| Time delay (msec) | 0 | 5 | 10 |
|---|---|---|---|
| Duration of core disassembly (msec) | 1.42 | 1.63 | 1.64 |
| Energy in the molten fuel (MWsec) | 1952 | 2142 | 2149 |
| Mass of molten fuel (%) | 76 | 79 | 79 |
| Average temperature of the molten fuel ($^{o}$C) | 3075 | 3120 | 3121 |

fraction criterion was used in the present work. The failure position was assumed to be at 47 % of the active core height, which corresponds to the position of the highest power density. These pessimistic assumptions on pin failure were used to make sure that the disassembly phase is reached.

As shown in Table 2, the first pin failure in channel 1 occurs at very similar conditions as predicted by CAPRI-2. However, the fuel-coolant interaction (FCI), as modeled by HOPE, proceeds somewhat differently. In channel 1, fuel ejection occurs within about 10 ms (Fig. 6), but then the pressure drop in the cavity, and back pressure-build up in the FCI zone (Fig. 7) prevent further ejection. The fuel-to-coolant ratio resulting from this model is somewhat lower than that predicted by CAPRI (Table 2). The FCI zone pressure, which leads to slug ejection (Fig. 8) and sodium voiding, reaches its maximum only after about 13 ms. This delay is in part due to the 10 ms fragmentation time assumed.

The power rise after failure of the channels 1 and 2 is relatively slow (Fig. 9). Only after channel 10 fails, too, the large void reactivity of this outer channel leads to a fast power increase. The other channels fail in a rapid sequence, and the accumulating void ramps drive the reactor into a superprompt critical state. At the switchover point to disassembly, defined when the pellet-averaged fuel temperature in the hottest node reaches about 3150°C, the inner channels 1 and 2 and the upper position of channel 10 are voided, which leads to a void reactivity of about 80 ¢. The reactivity and power conditions are more severe than in earlier simulations. This is mainly due to the positive fuel motion reactivity associated with the ejection process, which dominates over the sweep out reactivity in the voided channels. Thus, the fission gas pressure in the present model leads to fuel compaction with an associated positive reactivity in the pre-disassembly phase.

The pressure distribution in the core region at the beginning of the disassembly phase is shown in Table 3. High fission gas pressures are present in the unvoided nodes. However, in the voided portion of the core the gas can expand into the void space, and the pressures are rather moderate. For example, the cavity pressure of about 1000 bar in channel 1 (Fig. 7) reduces to about 15 bar, due to the expansion into the large void space. The disassembly calculation was carried out assuming that further fission gas release occurs in proportion to the melt fraction, without any time delay.

During the disassembly phase, the high pressures in the nodes next to the voided regions are relieved by an implosive motion. This is illustrated by looking at the pressure histories in the nodes 7 of channel 1 and channel 3 (Fig. 11 and 12), and at the distorted Lagrangian lattice at the end of the disassembly phase (Fig. 10). This motion, however, produces only small reactivity effects because of the low worth gradients. In the outer core region, there is a strong outward motion in radial direction, which, in combination with axial motions, produces the main shutdown effect. The relief proceeds rather smoothly. Single-phase pressures and the associated rapid oscillations, which were observed in the simulations for the fresh core /10/ cannot occur because of the cushioning effect of the fission gas.

Core disassembly proceeds more rapidly than in the CAPRI-KADIS simulation, leading to a considerably lower energy release. The energy in the molten fuel, 1952 MJ, is only 66 % of the earlier case (Table 2).

One may argue that in the HOPE-KADIS system the results depend sensitively on the swithover temperature to disassembly, because this temperature defines the point in time where the fission gas pressure becomes effective for core disassembly. This is indeed to be expected. However, the case under study is on the pessimistic side. In addition to a high switchover temperature the cavity pressures are high, and the clad rupture stress is exceeded over a large portion of the core and the reactor is prompt critical; thus, conditions for the validity of a disassembly model are certainly fulfilled.

In order to check the sensitivity of the results, a second case was run where the switchover temperature was lowered to 2800°C. It was found that the conditions at the beginning of the disassembly calculations are much less severe in this case. The normalized power is 752, and the pressure in the hottest KADIS node is about 300 bar. The KADIS calculation leeds to an energy in the molten fuel of 983 MJ, which is only 50 % of the original case. This result demonstrates that the high switchover temperature in the original case is a pessimistic assumption.

It was pointed out by Jackson /19/ that the effect of fission gas pressure as a shutdown mechanism in prompt-critical excursion may be lost if the gas release from the melting fuel occurs only with a time delay. It should

be noted that the time scale in which gas is released is not well known, though a first estimate published by Ostensen /20/ indicates that it is small. To check the influence of such a time delay on the accident under study, additional KADIS cases were run, where gas release is assumed to be delayed by 5 msec, and by 10 msec. The results are quoted in Table 4. The resulting energy in the molten fuel is only about 10 % higher in the case with a delay time, and still below the value of the CAPRI-2/KADIS simulation. The results are so insensitive to the delay time because in this simulation, most of the gas release occurs during the predisassembly phase, where heating is much slower, and the release less sensitive to time-delay effects. It is actually the gas present in the cavity at the disassembly point which blows the core apart. This situation is clearly different from the one investigated by Jackson /19/, where the gas release occurs during the prompt critical phase.

Fission gas influences the course of this accident in two characteristic ways. In the fuel ejection model the gas pressure acts as a driving force for autocatalytic fuel compaction towards the axial midplane. Thus, more severe conditions are predicted at the end of the predisassembly phase. On the other hand, the fission gas pressures cause core disassembly at relatively low fuel enthalpies, and thus lead to reduced energy release. The present models are consistent, because they take account of both effects. Though both effects may possibly be overestimated, the tendency towards a lowering of the energy release is clearly demonstrated.

## 5.2 Results obtained with Different Assumptions for the Transient Fission Gas Release Using a Mechanical Failure Criterion

To define pin failure at a certain melt fraction is a somewhat arbitrary procedure, based on melt fractions at which failure was observed in experiments. However, the code HOPE allows a more detailed modeling of the phenomena which lead to pin failure, the sequence being gas release as a consequence of the melting of unrestructured fuel, pressurization of the cavity, which loads the clad via a strengthless fuel after being reduced with the ratio of the transient melt and inner clad radii. Failure is predicted at time and position where the clad hoop stress first exceeds the rupture stress. Evidently, the clad stress is a more direct indicator of pin failure than a melt fraction.

Table 5: Results for the TOP cases T1 and T2

| Case | T1 | T2 |
|---|---|---|
| Ramp Rate ($/sec) | 0.15 | 0.15 |
| Gas Release at the Solidus | 20 % | 100 % |
| Failure Criterion | burst stress | |
| Failure Time (sec) | 9.37 | 9.21 |
| Normalized Power | 4.8 | 4.7 |
| Cavity Pressure (bar) | 818 | 725 |
| Failure Position (% of active core height) | 61 % | 61 % |
| Data at switch over | | |
| Time (sec) | 9.42 | 9.29 |
| Normalized Power | 412 | 570 |
| Net Reactivity and Ramp ($;$/sec) | 1.009/3 | 1.050/5 |
| Void Reactivity and Ramp ($;$/sec) | 1.288/38 | 1.165/50 |
| Fuel Reactivity and Ramp ($;$/sec) | -0.482/-6 | -0.273/-11 |
| Doppler Reactivity and Ramp ($;$/sec) | -1.236/-29 | -1.238/-34 |
| Results from Disassembly Calculations | | |
| Duration (msec) | 1.50 | 1.47 |
| Energy of molten fuel (MWsec) | 1101 | 1137 |
| Mass of molten fuel (kg) | 3111 | 3188 |

Two simulations of a 15 ¢/sec ramp accident, using this failure criterion were studied and reported in an earlier publication [7]. The important results will be repeated here. In the first case, T1, the standard parameters for gas release were used, which correspond to 20 % release at the solidus, and 80 % in proportion to the melt fraction. However, as mentioned in Section 2.2, one expects that in a slow transient a large fraction of gas is released by the time the fuel reaches the melting point. Without attempting any detailed modeling, this behavior was simulated in case T2 by assuming 100 % gas release at the solidus.

In case T1, the rather low powered channel 9 is the first to fail; this is because the volume of the central channel is small, and thus the gas release leads to a rather high cavity pressure. The FCI has time to void large portions of the channels 9 and 3. At switch over, the core is characterized by a much lower power than in the case with a thermal criterion, and the accident is much milder, with an energy in the molten fuel of 1101 MWs after disassembly (Table 5 and Fig. 14).

In case T2, gas release and cavity pressurization occur immediately after melting of unrestructured fuel. Thus, failure occurs at a smaller enthalpy content of the fuel, and the time period from failure to disassembly becomes somewhat extended. However, the general accident sequence, and especially the disassembly phase is rather similar to case T1; the energy in the molten fuel is only about 4 % higher.

Thus, it has been shown that the use of a mechanical failure criterion leads to a reduced predicted energy release, as compared to a thermal failure criterion. The two reasons are that failure occurs at a higher axial position, and that the failure sequence is not as coherent. In addition, these simulations show that early gas release does not represent a mechanism which leads to a more coherent failure of the channels.

## 5.3 Influence of the New Equation of State SSTEOS on a TOP Accident in the Fresh Core

As reported in Section 4.2 the new equation of state SSTEOS for $UO_2$ was introduced in the disassembly code KADIS. It includes more recent experimental information [11] than the ANLEOS, which was used in earlier studies [10].

To assess the influence of these new data on the disassembly simulation, a 5 $/s ramp accident in the fresh Mark 1A core of the SNR 300 was selected. Though this case is not of central importance, and was studied earlier only in the course of parameter variations /10/, it was taken for this study because one expects a large influence of the equation of state data in the case of a high initiating ramp rate.

The two equations of state are different mainly in two points:

- The vapor pressure in SSTEOS is about 60 % higher than in ANLEOS. It was however, demonstrated by Fröhlich et al. [10] that increasing the vapor pressure by 100 % reduces the energy release only by about 10 %. Therefore, a case was selected for this study where the vapor pressure is not the main shutdown mechanism.

- The liquid density in SSTEOS is characterized by a density change of 9.6 % upon melting, and a coefficient of thermal expansion $\alpha_\ell = 12.7 \cdot 10^{-5}/^{\circ}C$ for liquid $UO_2$. The former value is taken from experiment [12], the latter is predicted by the model, and is 20 % above the experimental value [11]. The corresponding data in the ANLEOS are 3.7 %, and $\alpha_\ell = 7.3 \cdot 10^{-5}/^{\circ}C$. This difference in the liquid density plays an important role in the 5 $/s TOP case, where single-phase pressures provide the major shutdown mechanism.

The results of the KADIS calculations with the two equations of state are shown in Table 6. KADIS allow to account for heat transfer from fragmented fuel to sodium above a certain threshold temperature (usually 2705°C). Cases with and without heat transfer ("with FCI" and "without FCI") were studied. The input data for all the four cases are from the same simulation of the predisassembly phase by CAPRI-2. The case "ANLEOS, with FCI" was quoted by Fröhlich et al. [10]. Both with and without FCI, use of SSTEOS leads to a faster shutdown, and to lower energy release, than ANLEOS.

Thus, the ANLEOS leads to pessimistic results mainly because the assumed liquid density is too high, whereas it was shown earlier [10] that the magnitude of the vapor pressure has relatively little influence on the results.

Table 6: Results of KADIS Calculations with different Equations of State for $UO_2$ SNR-300, Mark IA, Ramp Rate 5 $/sec

| | With FCI | | Without FCI | |
|---|---|---|---|---|
| | ANLEOS | SSTEOS | ANLEOS | SSTEOS |
| At Disassembly Begin: | | | | |
| Net Reactivity ($) | 1.114 | 1.114 | 1.114 | 1.114 |
| Net Reactivity Ramp ($/s) | 21.7 | 21.7 | 21.7 | 21.7 |
| Doppler-Ramp ($/s) | -51.9 | -51.9 | -51.9 | -51.9 |
| Results of Disassembly calculation: | | | | |
| Duration of Disassemblyphase (ms) | 2.34 | 1.94 | 3.15 | 2.60 |
| Energy of molten fuel (MWs) | 2288 | 1615 | 4910 | 2887 |
| Mass of molten fuel (%) | 78 | 66 | 96 | 82 |
| Mean temperature of molten fuel (K) | 3495 | 3248 | 4356 | 3594 |

It should be mentioned that the equation of state SSTEOS was evaluated for $UO_2$, and can be applied to (U, Pu)$O_2$ only as an approximation. However, the liquid fuel density at the melting point was adjusted to the (U,Pu)$O_2$ density used in the CAPRI-2 simulation of the predisassembly phase. Thus, the data used in the two codes were consistent.

## Conclusions

The accident analysis codes HOPE and KADIS, which are linked by an automatic data transfer system, provide an important tool to estimate the energy release in unprotected transient overpower (TOP) accidents, if assumptions are so pessimistic that the accident terminates in a hydrodynamic core disassembly. The codes allow a consistent treatment of fission gas effects both in the predisassembly phase (HOPE), and the disassembly phase (KADIS) of the accident.

The energy release predicted for a TOP accident in the end-of-life core of the SNR-300 remains on an acceptable level even for a pessimistic thermal failure criterion, and failure position. In fact, the energy release is lower than the one obtained in an earlier analysis with the codes CAPRI and KADIS. These results bear out the earlier conclusions that fission gas pressure provides an important shutdown mechanism in reactivity-ramp induced superprompt critical accidents [17].

The application of a more realistic mechanical failure criterion further leads to a substantial reduction in energy release in a mild transient. The present TOP analyses, which are based on the discussed modelling of fission gas effects, are considered to be an important step toward the removal of unnecessary conservatism in hypothetical reactivity ramp accidents.

## Appendix A. Calculation of the Speed of Sound in Liquid $UO_2$

Jackson and Nicholson [17] derived the following expression for the speed of sound, $c_f$, in single-phase liquid $UO_2$ (eq. (A.10))

$$c_f^2 = v^2 \frac{p\left(\frac{\partial F_2}{\partial U}\right)_{vr} \left(\frac{\partial F_2}{\partial v_r}\right)_U \left(\frac{\partial F_3}{\partial v}\right)_{\rho s}}{1 - \left(\frac{\partial F_2}{\partial v_r}\right)_U \left(\frac{\partial F_3}{\partial \rho_s}\right)_v \frac{dF_4}{dp}}$$

where $F_3$ and $F_4$ refer to sodium data, so that only the derivatives of $F_2$ must be redefined in terms of the new SSTEOS.

One finds

$$p = F_2(U,v_r) = p_{sat}(\rho_r) + \frac{1}{c_v}\left(\frac{\partial p}{\partial T}\right)\left[U-U_{sat}\right]$$

$$\left(\frac{\partial F_2}{\partial U}\right)_{v_r} = \frac{1}{C_v(\rho_r)} \frac{\partial p}{\partial T}(\rho_r)$$

$$\left(\frac{\partial F_2}{\partial v_r}\right)_U = -\rho_r^2 \frac{\partial F_2}{\partial \rho_r}$$

$$\left(\frac{\partial F_2}{\partial \rho_r}\right)_U = \frac{\partial p_{sat}}{\partial \rho_r} + (U-U_{sat}) \frac{1}{C_v} \frac{d}{d\rho_r}\left(\frac{\partial p}{\partial T}\right) - (U-U_{sat}) \frac{1}{C_v^2} \frac{\partial p}{\partial T} \frac{dCv}{d\rho_r}$$

$$- \frac{1}{C_v} \frac{\partial p}{\partial T} \frac{dU_{sat}}{d\rho_r}$$

where

$$\frac{\partial p_{sat}}{\partial \rho_r} = \frac{dp_{sat}}{dT_{sat}} \frac{dT_{sat}}{d\rho_r}$$

$$\frac{\partial U_{sat}}{\partial \rho_r} = \frac{0.535077}{\sqrt{1-0.4664\times10^{-4}(T_{sat}-3120)}} \cdot \frac{dT_{sat}}{d\rho_r}$$

The different derivatives are given by

a) $\rho_r > 2.747$

$$\frac{dT_{sat}}{d\rho_r} = \left[-1463.4+178.28(5.27-\rho_r)\right] \frac{7550-Tm}{4430}$$

$$\frac{dC_v}{d\rho_r} = 8.69154\times10^{-3}+5.76128\times10^{-3}(5.27-\rho_r)$$

$$\frac{d}{d\rho_r}\left(\frac{dp}{dT}\right) = 39.66-15.646(5.27-\rho_r)$$

b) $\rho_r < 2.747$

$$\frac{dT_{sat}}{d\rho_r} = \left[-1611.2(\rho_r-1)+649.32(\rho_r-1)^2\right] \frac{7550-Tm}{4430}$$

$$\frac{dC_v}{d\rho_r} = 6.43881\times10^{-3}+3.21863\times10^{-3}(\rho_r-1)$$

$$\frac{d}{d\rho_r}\left(\frac{dp}{dT}\right) = 4.698(\rho_r-1)-0.7236(\rho_r-1)^2$$

## Appendix B. Input Description for HOPE

A major portion of the input is specified using namelist dictionaries. Only large arrays (e.g. reactivity coefficients) are independently specified. Note that the main time step for the thermohydraulics calculation is an input quantity; for control, see ISTEP. The neutron kinetics time step size, which is much smaller, is controlled by the program; the initial value is an input quantity.

### Namelist NAM1

| | |
|---|---|
| NDG | Number of delayed neutron groups ($\leq$ 6) |
| MZC | Number of axial coolant nodes for each channel ($\leq$ 30) |
| MZF | Number of axial fuel nodes for each channel ($\leq$ 20) |
| NR | Number of channels ($\leq$ 13) |
| NS | Number of radial fuel nodes ($\leq$10) |
| JOT | Number of main time steps between full printouts |
| ISTEP | 0 The main time step is equal to HTEMP throughout the run<br>1 The main time step switches from HTEMP to SHTEMP at the switch point<br>2 The same as 1; in addition, the main time step before the switch point is slightly reduced if the power is high |

| | |
|---|---|
| JOTS | Number of main time steps between full printouts after the switch point |
| TFMAX | Maximum fuel node temperature (K); terminates the run |
| PFMAX | Maximum normalized power; terminates the run |
| PFMIN | Minimum normalized power; terminates the run |
| NREG | Number of geometrical regions (either 1 or 2). A geometrical region is composed of all fuel pins of one type. NREG=3: The quantities TIME, TR2 (= main time step), PJ1 (= normalized power) are read in from the external unit 9. This option is suitable if the power transient is pre-specified. The number of geometrical regions is two. |
| KRAD | Number of channels for which the fuel pin radial geometry is specified in the input ($1 \leq KRAD \leq NR$). The input data are used for channels 1 to KRAD-1 and NR. For any remaining channels, input data specified for KRAD-1 are used. |
| MZBU | Number of upper axial blanket nodes. |
| MZBD | Number of lower axial blanket nodes. |
| NOP | Number of main time steps after which abbreviated printouts are printed after the switch point. |

| | |
|---|---|
| IBLANK | 1 |
| KUEB | 1 Transfer data are prepared and stored on an external unit<br>0 Transfer data are not prepared |

Namelist NAM2

| | |
|---|---|
| STEP | Input reactivity step ($) |
| RAMP | Input reactivity ramp ($/sec) |
| ACCELN | Input reactivity acceleration ($/sec$^2$) |
| EPS1 | Maximum error for kinetics routine |
| HO | Initial neutron kinetics time step size |
| TMAX | Real time for run termination (sec) |
| PO | Initial steady state core power (MW) |
| TP | Prompt neutron lifetime (sec) |
| BETATL | Total delayed neutron fraction |
| BETA | Delayed neutron group fractions (Dimension NDG) |
| DLAMBA | Delayed neutron group decay constants (sec$^{-1}$) (Dimension NDG) |

| | |
|---|---|
| HTEMP | Initial main time step size (sec) |
| SWTEMP | Switch point central fuel temperature in the hottest node |
| SHTEMP | Main time step size after switch point (SEC) |
| SWPRES | Switch point fuel pin cavity pressure (at) |
| SWMF | Switch point fuel melt fraction |
| SWTAV | Switch point axial node average fuel temperature (K) |
| SWHOOP | Switch point clad hoop stress (fraction of ultimate stress) |
| SWCTEM | Switch point clad temperature (K) |
| DTIME | Time interval for the reactivity table after the switch over point |

Namelist NAM3

| | |
|---|---|
| AK<br>BK<br>CK | Constants for the fuel thermal conductivity equation |
| PCROS | Average porosity of the fuel |
| CSC | Average thermal conductivity of the clad (W/cm-K) |
| CPF | Heat capacity of the fuel for steady state calculation (W-sec/g-K) |

| | |
|---|---|
| FHF | Heat of fusion of the fuel (J/g) |
| GAM2 | Ratio of the structure surface area to clad surface area |
| GAMC | Fraction of the power produced in the coolant |
| HBCON | Coefficient in the bond-conductance equation when a gap exists (Conductance = HBCON/GAP) (W/cm-K) |
| HBMAX | Maximum value of the bond conductance ($W/cm^2$-K) |
| GAMS | Fraction of the power produced in the clad |
| CII, C22, C33 | Convection heat transfer coefficients |
| TO | Steady state coolant inlet temperature (K) |
| PLP | Length of inlet plenum (cm) |
| AR | Area ratio for pump leg (Diameter of pump leg)$^2$/(Diameter of coolant channel)$^2$ |
| PLHG | Length of coolant plenum above core (cm) |
| ZPL | Height of the bottom of the lower axial blanket (Normally set to 0 and called the reference height) (cm) |

| | |
|---|---|
| VFC | Volume fraction of the coolant (First geometrical region) |
| PX | Upper plenum cover pressure (at) |
| EPS2 | Not in use |
| TAUM | (Structure volume)/(Structure area in contact with the coolant) |
| RHOCPM | Density times specific heat of the clad and structure (W-sec/$cm^3$-K) |
| CLC | Average thermal conductivity of the coolant (W/g-K) |
| RSM | Thermal resistance of the structure (cm-K/W) |
| ROC | Outer radius of the fuel pin (cm) |
| TPMELT | Fuel melting temperature |
| SBCTE | Stefan-Baltzmann constant times emissivity for fuel-clad radiant heat transfer ($W/cm^2-K^4$) |
| AFS | Fuel solid expansion coefficient (Dimension 3) for the 3 fuel restructuring regions |
| AFM | Fuel melting expansion coefficient (Dimension 3).If AFM (3) > 1, it is calculated by code |
| AFL | Fuel liquid expansion coefficient (1/K) |

| | |
|---|---|
| AFC | Clad solid expansion coefficient (1/K) |
| TREF | Initial reference temperature for computing clad and fuel thermal expansion (K) |
| FRC | Single phase coolant friction coefficient |
| FTFOT | Fuel density relativ to the theoretical density (dimension 3) |
| ROB | Outer radius of the second geometrical region fuel pins (cm) |
| VFB | Volume fraction of the coolant in the second geometrical region |
| GPMX | Maximum gap width for use in the fuel-clad conductance equation (cm) |
| IDTYP | Fuel restructing flag (dimension NR) |
| | 1 Fuel is restructured. |
| | 2 Fuel is not restructured. |

Namelist NAM4

| | |
|---|---|
| GASF | Mass of fission gas produced per atom % burnup per unit mass of fuel |
| RG | Gas constant for the fissiongas ($atcm^3/gK$) |
| TCOL | Temperature above which fuel restructures to columnar grains (K) |
| TEQX | Temperature above which fuel restructures to equiaxed grains (K) |
| TLOW | Not in use |
| PCAV | Initial fuel pin center void pressure (at) (Dimension NR) |
| BURNUP | Peak burnup of each channel (Dimension NR) |
| VLPN | Volume of the fission gas plenum per pin ($cm^3$) |
| GGBF | Fraction of the fission gas on the grain boundaries at the start of the transient |
| BMF | Bulk modulus of molten fuel (1/at) |
| PXCRT | Fission gas critical pressure (at) |
| TXCRT | Fission gas critical temperature (K) |
| VXCRT | Fission gas critical specific volume ($cm^3/g$) |

| | |
|---|---|
| ISTYP | Fraction times 10 of the elastic limit stress initially present in the clad |
| CSMAX | Maximum allowable clad strain (fraction) |
| CYM | Effective clad Young's Modulus (at) |
| GAC | Fission gas ratio of specific heats |
| IRTYP | 2 (standard case) Dutt model used for fission gas release. Release in columnar grain and equiaxed fuel are input values (usually equal to one)<br>1 release in unrestructured fuel is zero |
| ICTYP | 1 center void and fission gas plenum in pressure equilibrium<br>0 no communication between center void and plenum |
| FYM | Effective fuel Young's modulus (at) |
| CUE | Clad (plastic) strains associated with the ultimate stress |
| CUS1<br>CUS2 | Clad burst stress formula coefficients |
| CYS1<br>CYS2 | Clad yield stress formula coefficients |
| SURT | Surface tension for fission gas bubbles in fuel-fission gas emulsion (dyne/cm) |

| | |
|---|---|
| RBUB | Fission gas bubble radius for fuel-fission gas emulsion (A) |
| SFAC1 | Fraction of fission gas retained in columnar fuel (dimension NR) |
| SFAC2 | Fraction of fission gas retained in equiaxed fuel (dimension NR) |

Namelist NAM5
(pin failure criteria)

| | |
|---|---|
| TIFAIL | Equal TPMELT; unrestructured melt criterion |
| INF | not in use |
| TFAIL | Average axial fuel node temperature (K) |
| TCFAIL | Clad temperature (K) |
| UFAIL | Fuel melt fraction |
| PFAIL | Cavity pressure (at) |
| YFAIL | ≥0: clad hoop stress (fraction of burst stress)<br><0: clad plastic strain |
| IFM | Specifies the failure criterion used (dimension NR)<br>6 cavity pressure criterion<br>5 hoop stress or clad strain criterion<br>4 melt fraction criterion<br>3 clad temperature criterion |

| | |
|---|---|
| | 2 average axial fuel node temperature criterion<br>1 unrestructured melt criterion<br>0 all failure criteria used |
| CTL | Length of clad failure (dimension NR) |
| CTW | Width of clad failure (dimension NR) |
| NB | Failure location criterion (dimension NR)<br>0 failure node found by YFAIL failure criterion<br>100≤NB<200: failure node NB-100<br>200≤NB<300: failure node 200-NB+uppermost molten fuel node<br>NB≥300: failure node NB-300+lowermost molten fuel node |
| EFC | Ejection friction coefficient for use in the time dependent Bernoulli equation |
| SLIP | Fission gas to molten fuel ejection velocity ratio |

Namelist NAM6

| | |
|---|---|
| PR | Initial ejected molten fuel particle radius (cm) |
| PRS | Initial ejected solid fuel particle radius (cm) |
| FFRAC | Fraction of coolant flow cross section area which remains as a liquid film |

| | |
|---|---|
| TAUFG | Fragmentation time (sec) |
| ZTOP | Height of the top of the upper sodium column (cm) |
| ZBOT | Height of the bottom of the lower sodium column (cm) |
| IFTYPE | 1 no fragmentation<br>2 normal fragmentation model |
| NFRS | Number of fragmentation steps for complete fragmentation |
| VDNOF | Interaction zone void fraction fragmentation cutoff |
| SCOF | Interaction zone degree of subcooling fragmentation cutoff |
| IFHTYP | Fission heating of ejected particles,<br>1 fission heating included<br>0 fission heating not included |
| HCOND | Condensation heat transfer coefficient for condensation of coolant vapor on clad (W/cm-K) |
| TAUNFG | Fuel expulsion group time period when fragmentation is not occuring (sec) |
| ISFRG | 0 no solid particle fragmentation (standard case)<br>1 solid particle fragmentation included |

Namelist NAM7

| | |
|---|---|
| CDP | Drag coefficient used for high Reynolds number conditions when calculating fuel motion from sodium drag force (CDP=.44 normally) |
| NPG | Number of particle size groups for describing each fuel expulsion group ($\leq 3$) |
| NCG | Number of cell interfaces for determining fuel motion cells ($\leq 5$) |
| PDS | Radius of each particle size group (dimension NPG) |
| PDW | Fraction of total mass of each particle size group (dimension NPG) |
| PCW | Fraction of total mass of each particle size group in each fuel motion cell (dimension (NCG-1)·NPG) |
| PPFDW | Partial fragmentation fractions of the total mass of each particle size group (dimension 2·NPG) |

Input Arrays

| | |
|---|---|
| ZCOOL(1), ZCOOL(MZC) | Height of the bottom of the lowest, and top of the highest axial coolant node (cm) (FORMAT1OF8.3) |

The following arrays have FORMAT6E12.4

| | |
|---|---|
| ((DOPLER(J,K),J=1,MZF),K=1,NR) | Weight fraction of Doppler term proportional to $T^{-1}$ in each axial fuel node (sum over nodes in each channel equals 1) |
| ((WDOP3(J,K),J=1,MZF),K=1,NR) | Weight fraction of Doppler term proportional to $T^{-3/2}$ in each axial fuel node (sum over nodes in each channel equals 1) |
| (ADOP(K),K=1,NR) | Doppler term $\sim T^{-1}$ for each channel (sodium in) |
| (BDOP(K),K=1,NR) | Doppler term $\sim T^{-1}$ for each channel (sodium out) |
| (ADOP3(K),K=1,NR) | Doppler term $\sim T^{-3/2}$ for each channel (sodium in) |
| (BDOP3(K),K=1,NR) | Doppler term $\sim T^{-3/2}$ for each channel (sodium out) |
| (G1(K),K=1,NR) | Channel steady state coolant mass flow ($g/cm^2$-sec) |
| (ZFL(J),J=1,MZF+1) | Axial fuel node coordinate (cm) (ZFL(1)=O) |
| (PINNO(K),K=1,NR) | Number of pins in each channel |

| | |
|---|---|
| ((PFAC(J,K),J=1,MZF),K=1,NR) | Fraction of total power in each axial node |
| ((VOID(J,K),J=1,MZF),K=1,NR) | Sodium worth in each axial node ($\delta k/k$) |
| ((FUEL(J,K),J=1,MZF),K=1,NR) | Fuel worth in each axial node ($\delta k/k$) |

The following arrays for the fuel pin radii R must be prepared for KRAD channels:

| | |
|---|---|
| (R(1,J,K),J=1,MZF) | center void radius |
| (R(NT,J,K),J=1,MZF) | outer fuel radius |
| (R(NU,J,K),J=1,MZF) | inner clad radius |
| (R(NV,J,K),J=1,MZF) | outer clad radius |

End of input

Note that the Doppler coefficient for each channel K is assumed to be given by

$$\frac{ADOP(K)}{T} + \frac{ADOP3(K)}{T^{3/2}} \quad \text{for sodium-in condition}$$

$$\frac{BDOP(K)}{T} + \frac{BDOP3(K)}{T^{3/2}} \quad \text{for sodium-out condition}$$

Within each channel, the fraction of the Doppler coefficient associated with the axial node J is

DOPLER(J,K) for the term $\sim T^{-1}$

WDOP3(J,K) for the term $\sim T^{-3/2}$

If a node is partially void, the code interpolates between "wet" and "dry" conditions.

## Appendix C. HOPE Input for a Sample Problem

In this Appendix, the job control cards and the input data for a HOPE sample problem will be given. The 15 ¢/sec ramp accident discussed in Section 5.1 is selected as an example.

The job control cards are:

```
//INR528KU JOB (0528,101,P6N1E),ARNECKE,REGION=544K,TIME=(20,00)
//*MAIN LINES=20
// EXEC FHG,LIB=NUSYS,NAME=HOPE
//G.FT09F001 DD DUMMY
//G.FT20F001 DD UNIT=2314,VOL=SER=GFK016,DSN=HOPE15.INR528,
// DISP=(,KEEP),SPACE=(TRK,10,RLSE),DCB=(BLKSIZE=7200,RECFM=VBS)
//G.FT21F001 DD UNIT=3330,VOL=SER=KAPROS,DISP=(,KEEP),
// DSN=FISCHER.REAKTBL,DCB=(RECFM=VBS),SPACE=(TRK,5,RLSE)
//G.FT10F001 DD UNIT=2314,VOL=SER=GFK016,DSN=SPL1.INR107,
// DCB=(LRECL=X,BLKSIZE=1680,RECFM=VBS),SPACE=(TRK,(10,5),RLSE),
// DISP=(,KEEP)
//G.FT11F001 DD UNIT=2314,VOL=SER=GFK016,DSN=SPL2.INR107,
// DCB=(LRECL=X,BLKSIZE=1680,RECFM=VBS),SPACE=(TRK,(10,5),RLSE),
// DISP=(,KEEP)
//G.SYSIN DD DSN=TSO107.HOPE.DATA,DISP=SHR
```

Note that in this case the plot data are stored on units 10 and 11, the transfer data on unit 20, and the reactivity table on unit 21.

The option to write the power history on unit 9 is not used; therefore, the DD statement is replaced by a DUMMY statement.

The NAMLIST input data for this case are given in the following table.

Many of the input arrays were published in Ref. [10], see Tables 7.1.17 and 7.1.19-22 in the Reference. The remaining input arrays are specified in Tables C1 and C2 in this report. Note that the Tables in [10] have entries for 13 channels, but only the first twelve channels were used in the HOPE simulation. Note also that ZCOOL(1)=0, ZCOOL(MZC)= 180.4

Table. NAMLIST Input for HOPE

```
      0.15 $/SEC HOPE M1A  EOL CORE MELT FRACTION CRITERION
&NAM1 NDG=6,MZC=30,MZF=20,NR=12,NS=10,NREG=2,JOT=250,ISTEP=2,JOTS=250,KRAD=2,
TFMAX=3373.0,PFMAX=1.0E+06,PFMIN=0.950,MZBU=4,MZBD=3,NOP=200,IBLANK=1,KUEB=1,
&END
&NAM2 STEP=0.0000,RAMP=0.1500,ACCELN=0.0000,EPS1=0.0050000,HO=0.000010,
TMAX=12.0000,PO=7.5438E+08,TP=0.46210E-06,BETATL=3.03502E-3,
BETA=7.518E-5,6.7575E-4,5.6367E-4,1.1018E-3,4.6544E-4,1.5318E-4,
DLAMBA=0.012954,0.031311,0.13488,0.34404,1.3727,3.7691,
HTEMP=0.050,SWTEMP=5000.0,SHTEMP=0.0002,DTIME=0.002,
SWPRES=10000.,SWMF=0.290,SWTAV=3200.00,SWHOOP=1.300,SWCTEM=2000.00,&END
&NAM3 AK=-10.509,BK=0.06626,CK=-1.861E-05,POROS=0.135,CSC=0.2250,
CPF=0.662000,FHF=280.0000,TPMELT=3040.0,TAUM=0.2800,RSM=0.41000,GAMC=7.E-4,
HBCON=0.0150,HBMAX=0.80000,ROB=0.475,ROC=0.3000,VFB=0.3250,C11=0.02500,
C22=0.80000,C33=7.0000,TO=650.0,PLP=65.50,AR=1.000,PLHG=550.0000,
ZPL=00.00,GAMS=0.01100,VFC=0.50067,PX=1.5500,EPS2=0.000010,RHOCPM=4.7300,
GAM2=0.12864,SBCTE=4.57E-12,AFS=1.612E-05,1.612E-05,1.612E-05,
AFL=3.500E-05,AFM=2.000E-03,1.000E-03,1.000E+02,TREF=300.0,FRC=0.3740,
AFC=1.800E-05,FTFOT=0.95000,0.91000,0.86500,CLC=1.29070,GPMX=0.0100,IDTYP=1,1,
1,1,1,1,1,1,1,1,1,1,1,&END
&NAM4 GASF=1.281E-03,RG=0.626,TCOL=1973.0,TEQX=1575.0,TLOW=900.00,PCAV=20.0,
20.0,20.0,20.0,20.0,20.0,20.0,20.0,20.0,20.0,20.0,20.0,0.0,0.0,
BRNUP=7.65,7.6,7.5,7.27,7.25,7.11,6.94,6.9,6.51,7.54,6.14,0.0,0.0,
VLPN=14.140,GGBF=0.200,BMF=0.99E+06,PXCRT=58.0,TXCRT=290.0,VXCRT=0.917,
ISTYP=0,CSMAX=0.0200,CYM=8.00E+05,GAC=1.660,IRTYP=2,ICTYP=1,FYM=1.20E+06,
CUE=0.02,CUS1=13159.0,CUS2=9.050,CYS1=10390.00,CYS2=6.920,SURT=525.00,
RBUB=1500.00,SFAC1=1.00,1.00,1.00,1.00,1.00,1.00,1.00,1.00,1.00,1.00,
1.00,1.00,1.00,
SFAC2=1.00,1.00,1.00,1.00,1.00,1.00,1.00,1.00,1.00,1.00,1.00,1.00,1.00,&END
&NAM5 TIFAIL=3040.0,INF=1,TFAIL=3100.0,TCFAIL=1400.0,UFAIL=0.300,YFAIL=-0.01,
PFAIL=100.0,IFM=4,4,4,4,4,4,4,4,4,4,4,4,4,
CTL=5.00,5.00,5.00,5.00,5.00,5.00,5.00,5.00,5.00,5.00,
5.00,5.00,5.00,CTW=0.200,0.200,0.200,0.200,0.200,0.200,0.200,0.200,0.200,
0.200,0.200,0.200,
0.200,EFC=0.900,SLIP=1.000,NB=109,109,110,110,110,110,110,110,110,110,
110,110,110,&END
&NAM6 PR=0.1000,PRS=0.10000,FFRAC=.18,TAUFG=0.00125,ZTOP=550.000,ZBOT=-387.,
IFTYPE=2,NFRS=4,VDNOF=0.500,SCOF=5.0000,IFHTYP=1,HCOND=6.3,TAUNFG=0.005,
ISFRG=0,&END
&NAM7 CDP=0.440,NPG=3,NCG=5,PDS=0.500,0.12500,0.06250,PDW=0.300,0.5000,0.2000,
PCW=0.2500,0.2500,0.2500,0.2500,0.2500,0.2500,0.2500,0.2500,0.250,0.250,0.250,
0.2500,PPFDW=1.00,0.00,0.00,0.300,0.700,0.000,&END
```

Table C1 Input Arrays for HOPE

| Channel | Coolant Mass Flow G1 ($g/cm^2$-sec) | Number of Pins |
|---|---|---|
| 1 | 353.0 | 166 |
| 2 | 353.0 | 996 |
| 3 | 353.1 | 1494 |
| 4 | 325.5 | 1992 |
| 5 | 325.3 | 4930 |
| 6 | 305.8 | 2988 |
| 7 | 298.6 | 3984 |
| 8 | 296.0 | 2988 |
| 9 | 285.6 | 2988 |
| 10 | 351.2 | 6972 |
| 11 | 303.8 | 7968 |
| 12 | 121.2 | 5856 |

| Axial Node | Axial Fuel Node Coordinate (cm) |
|---|---|
| 1 | 16.08 |
| 2 | 32.16 |
| 3 | 40.18 |
| 4 | 48.21 |
| 5 | 56.23 |
| 6 | 64.25 |
| 7 | 72.28 |
| 8 | 80.30 |
| 9 | 88.32 |
| 10 | 92.20 |
| 11 | 102.08 |
| 12 | 108.96 |
| 13 | 115.84 |
| 14 | 122.72 |
| 15 | 129.60 |
| 16 | 136.48 |
| 17 | 143.36 |
| 18 | 150.24 |
| 19 | 163.45 |
| 20 | 176.66 |

Table C2: Normalized Power Distribution for HOPE Input (EOL Core)

| Channel | 1 | 2 | 3 | 4 | 5 | 6 | 7 | 8 | 9 | 10 | 11 | 12 |
|---|---|---|---|---|---|---|---|---|---|---|---|---|
| Axial Node | | | | | | | | | | | | |
| 1 | .054 | .054 | .058 | .055 | .042 | .051 | .048 | .046 | .042 | .035 | .027 | .068 |
| 2 | .114 | .114 | .111 | .102 | .113 | .097 | .096 | .094 | .088 | .074 | .057 | .140 |
| 3 | .097 | .096 | .094 | .089 | .075 | .086 | .085 | .083 | .079 | .069 | .052 | .118 |
| 4 | .638 | .636 | .628 | .604 | .600 | .585 | .568 | .560 | .524 | .607 | .489 | .163 |
| 5 | .764 | .761 | .750 | .724 | .720 | .705 | .686 | .677 | .638 | .742 | .598 | .206 |
| 6 | .875 | .871 | .858 | .830 | .826 | .810 | .790 | .780 | .737 | .860 | .695 | .243 |
| 7 | .933 | .928 | .915 | .886 | .884 | .865 | .843 | .838 | .790 | .911 | .741 | .376 |
| 8 | .983 | .973 | .965 | .935 | .933 | .914 | .891 | .886 | .836 | .965 | .786 | .400 |
| 9 | 1.000 | .995 | .982 | .952 | .950 | .931 | .909 | .904 | .854 | .986 | .804 | .410 |
| 10 | .844 | .840 | .830 | .805 | .804 | .788 | .770 | .766 | .724 | .837 | .683 | .349 |
| 11 | .809 | .805 | .796 | .773 | .773 | .758 | .741 | .737 | .697 | .806 | .659 | .337 |
| 12 | .752 | .747 | .739 | .721 | .723 | .709 | .692 | .688 | .650 | .755 | .619 | .317 |
| 13 | .675 | .667 | .657 | .650 | .656 | .644 | .625 | .617 | .536 | .686 | .565 | .288 |
| 14 | .627 | .611 | .538 | .600 | .615 | .600 | .574 | .550 | .534 | .644 | .527 | .172 |
| 15 | .523 | .504 | .481 | .504 | .523 | .509 | .481 | .453 | .444 | .543 | .447 | .144 |
| 16 | .420 | .402 | .383 | .411 | .432 | .418 | .389 | .361 | .355 | .439 | .365 | .113 |
| 17 | .052 | .050 | .048 | .051 | .054 | .052 | .049 | .046 | .046 | .428 | .034 | .083 |
| 18 | .037 | .032 | .031 | .035 | .037 | .035 | .032 | .029 | .029 | .027 | .022 | .059 |
| 19 | .034 | .035 | .033 | .039 | .042 | .040 | .035 | .030 | .030 | .029 | .024 | .070 |
| 20 | .018 | .017 | .034 | .020 | .023 | .021 | .018 | .014 | .014 | .014 | .012 | .037 |

Appendix D. Variables of the HOPE Plot Data Files

1. Plot Array VPL1O(NRW), (NRW=1,124) for each time step:

| NRW | Variable | Definition |
|---|---|---|
| 1 | TIME | Accident time (sec) |
| 2 | PJ1/PØ | Normalized Power |
| 3 | RHOJ1 | Net Reactivity ($) |
| 4 | RHONPT | Input Reactivity ($) |
| 5 | RHODOB | Doppler Reactivity ($) |
| 6 | RHONB | Sodium Void Reactivity ($) |
| 7 | RHOFB | Fuel Motion Reactivity ($) |
| 8-20 | T2(1,9,K) | Center Fuel Temperature ($^{o}$C) |
| 21-33 | TAVEF(9,K) | Pellet-averaged Fuel Temperature ($^{o}$C) |
| 34-46 | T2(NS,9,K) | Fuel Surface Temperature ($^{o}$C) |
| 47-59 | T2(NS+1,9,K) | Clad Temperature ($^{o}$C) |
| 60-72 | TCN(9,K) | Sodium Temperature ($^{o}$C) |
| 73-85 | UF(9,K) | Fuel Melt Fraction |
| 86-98 | CPST(9,K) | Peak node clad plastic strain |
| 99-111 | SHOOP(9,K) | Peak node clad hoop stress (at) |
| 112-124 | PCAV(K) | Cavity pressure |

Note that the variables with index K are written for 13 channels (K=1,13). The index 9 stands for the axial peak node.

2. Plot Array VPL11(NRW), (NRW=1,190) for each time step after failure of channel 1:

| NRW | Variable | Definition |
|---|---|---|
| 1-10 | TFCI(K) | FCI time (sec) |
| 11-20 | PCAV(K) | Cavity pressure (at) |
| 21-30 | PS2(K) | FCI zone pressure (at) |
| 31-40 | VE2(K) | Ejection velocity (cm/sec) |
| 41-50 | TAVEFR(K) | Average temperature of the ejected fuel ($^{o}$C) |
| 51-60 | TS2(K) | Sodium temperature in the FCI zone ($^{o}$C) |
| 61-70 | FMT(K) | Mass of fuel in the FCI zone (g) |
| 71-80 | SMAT(K) | Mass of sodium in the FCI zone (g) |
| 81-90 | ZU2(K) | Upper phase boundary of the FCI zone (cm) |
| 91-100 | ZD2(K) | Lower phase boundary of the FCI zone (cm) |
| 101-110 | VDFR(K) | Thermodynamic void fraction in the FCI zone |
| 111-120 | HAFS(K) | Heat transfer coefficient fuel to coolant (W/g of sodium) |
| 121-130 | UU2(K) | Velocity of the upper phase boundary (cm/sec) |
| 131-140 | UD2(K) | Velocity of the lower phase boundary (cm/sec) |
| 141-150 | TF2(K) | Fuel temperature in the second expulsion group ($^{o}$C) |
| 151-160 | (1-DST/DSL*FVCOR) | Void fraction obtained from the volume balance |
| 161 | RHOJ1 | Net reactivity ($) |
| 162 | RHONPT | Input reactivity ($) |

| NRW | Variable | Definition |
|---|---|---|
| 163 | RHODOB | Doppler reactivity ($) |
| 164 | RHONB | Sodium void reactivity ($) |
| 165 | RHOFB | Fuel motion reactivity ($) |
| 166 | PJ1/PØ | Normalized Power |

Note that the variables with the index K are written for the channels 1 to 10 (K=1,10).

References

/1/ H.G. Bogensberger, E.A. Fischer, P. Schmuck,
"On the Equation of State of Mixed Oxide Fuel for the Analysis of Fast Reactor Disassembly Accidents"
Conf. on Fast Reactor Safety, Beverly Hills, California (1974)
CONF-740401, p.1333

/2/ D. Struwe, P. Royl, P. Wirtz, G. Angerer, E.A. Fischer,
"CAPRI - A Computer Code for the Analysis of Hypothetical Core Disruptive Accidents in the Predisassembly Phase"
IBID., p. 1525

/3/ P. Schmuck, G. Jacobs, G. Arnecke,
"KADIS - Ein Computerprogramm zur Analyse der Kernzerlegungsphase bei hypothetischen Störfällen in schnellen, natriumgekühlten Brutreaktoren"
KFK-2497 (1977)

/4/ E.T. Rumble,
"A Hypothetical Overpower Excursion Model for Liquid Metal-Cooled Fast Breeder Reactors"
Ph. D. Dissertation in Engineering, UCLA, California (1974)

/5/ H.E. Schmidt,
"Die Wärmeleitfähigkeit von Uran- und Plutonium-Dioxid bei hohen Temperaturen"
High Temp., High Pressure 3, 345 (1971)

/6/ D.S. Dutt et al.,
"A Correlated Fission Gas Model for Fast Reactor Fuels"
Trans. Am. Nucl. Soc. 15, 198 (1972)

/7/ H.G. Bogensberger, E.A. Fischer, P. Royl, G. Arnecke,
"Analysis of LMFBR Overpower Accidents, Including Fission Gas Effects in the Predisassembly and Disassembly Phase"
International Meeting on Fast Reactor Safety and Related Physics, Chicago, Illinois (1976)

/8/ E.A. Fischer,
"Analysis of Experimental Fission Gas Behavior Data in Fast Reactor Fuel"
KFK-2370 (1977)

/9/ W. Zimmerer,
"PLOTCP - Ein Fortran IV-Programm zur Erzeugung von Calcomp-Plot-Zeichnungen"
KFK-2081 (1975)

/10/ R. Fröhlich et al.,
"Analyse schwerer hypothetischer Störfälle für den SNR-300 Mark 1A Reaktorkern",
KFK-2310 (1976)

/11/ E.A. Fischer, P.R. Kinsman, R.W. Ohse,
J. Nucl. Mater. 59, 125 (1976)

/12/ J.A. Christensen,
J. Amer. Ceram. Soc. 46, 607 (1963)

/13/ R.A. Hein et al.,
J. Nucl. Mater. 25, 99 (1968)
L. Leibowitz et al.,
J. Nucl. Mater. 29, 356 (1969)

/14/ R.W. Ohse, P.G. Berrie, H.G. Bogensberger, E.A. Fischer,
J. Nucl. Mater. 59, 112 (1976)

/15/ M. Bober, H.U. Karow, K. Schretzmann,
Nucl. Technol. 26, 237 (1975)

/16/ R.L. Gibby et al.,
"Analytical Expressions for Enthalpy and Heat Capacity for Uranium-Plutonium Oxide",
HEDL-TME 73-60 (1973)

/17/ J.F. Jackson, R.B. Nicholson,
"VENUS-II, An LMFBR Disassembly Program"
ANL-7951 (1972)

/18/ J.R. Findlay et al.,
"Fast Reactor Safety Studies Using VIPER",
US/Japan Seminar on Fast Pulse Reactors, Jan. 1976

/19/ J.F. Jackson and A.M. Eaton,
"Pressurization Rate Effects in Irradiated-Core Disassembly Calculations",
Trans. Am. Nucl. Soc. 22, 370 (1975)

/20/ R.W. Ostensen,
"Fission Gas Bubble Modeling for LMFBR Accidents"
Trans. Am. Nucl. Soc. 26, 583 (1977)

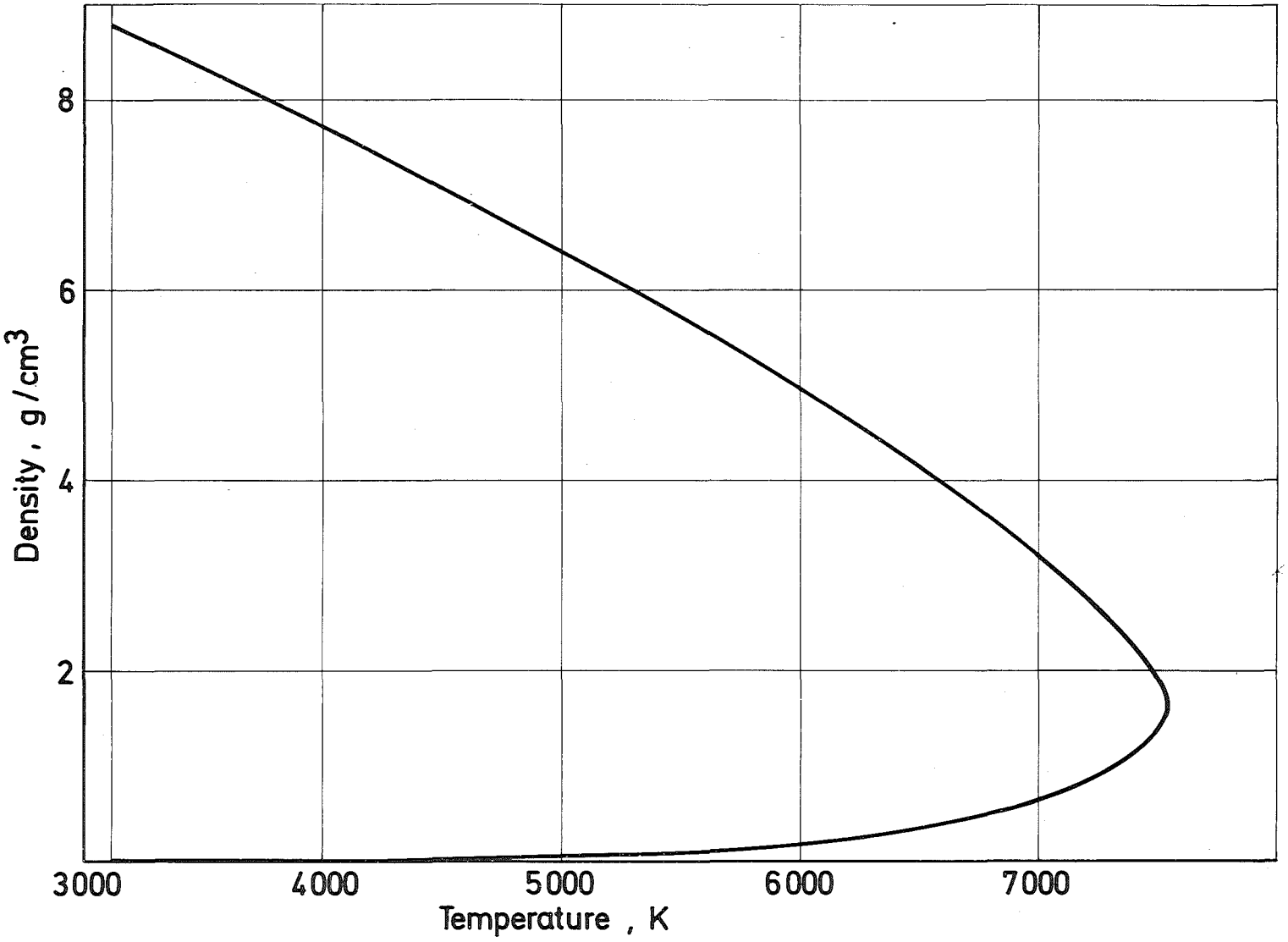


Fig. 1 Equation of State of $UO_2$: Density of the Saturated Liquid and Vapor

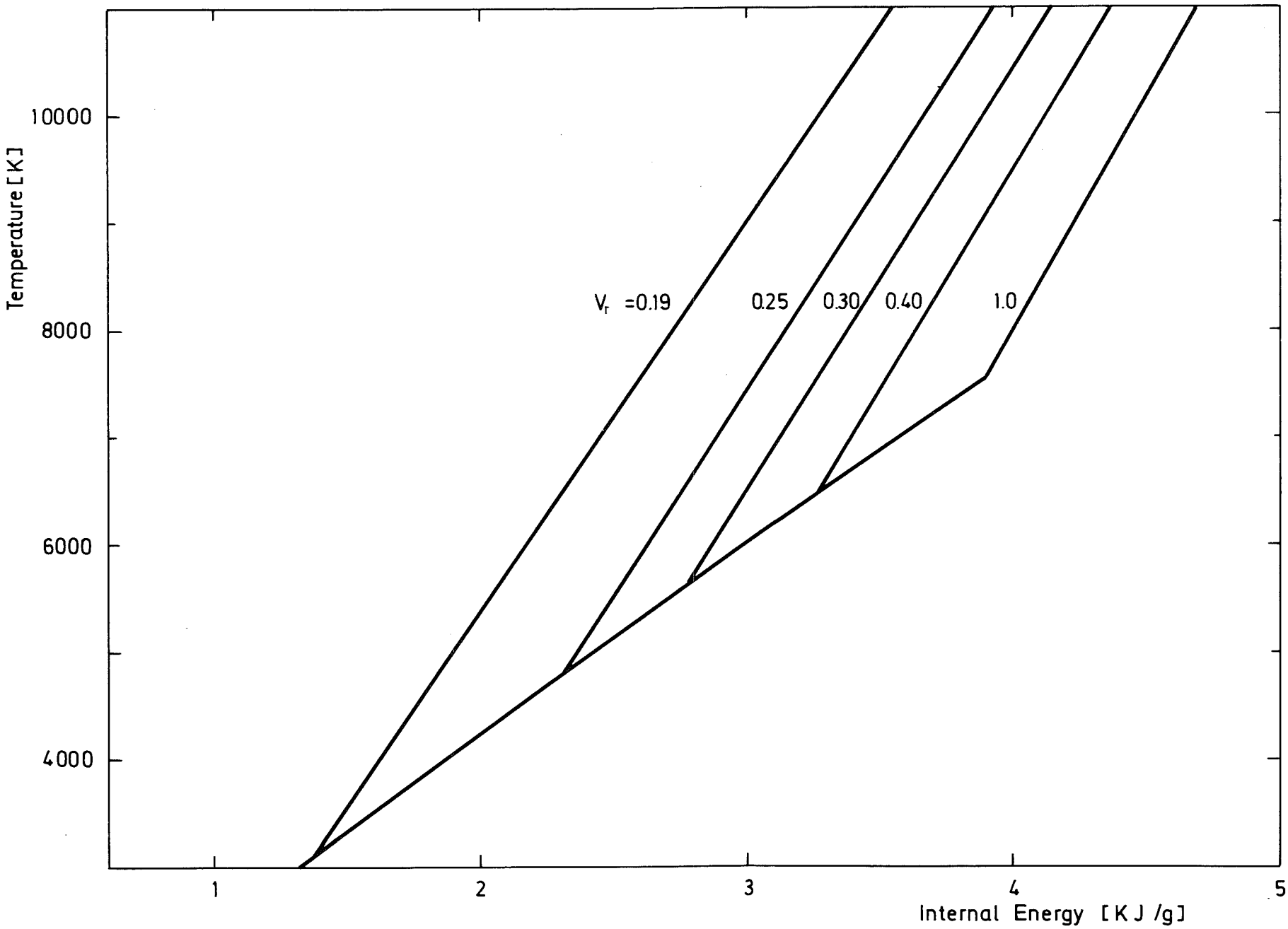


Fig. 2: Equation of State of $UO_2$: Temperature versus Internal Energy ($V_r$ = Reduced Specific Volume)

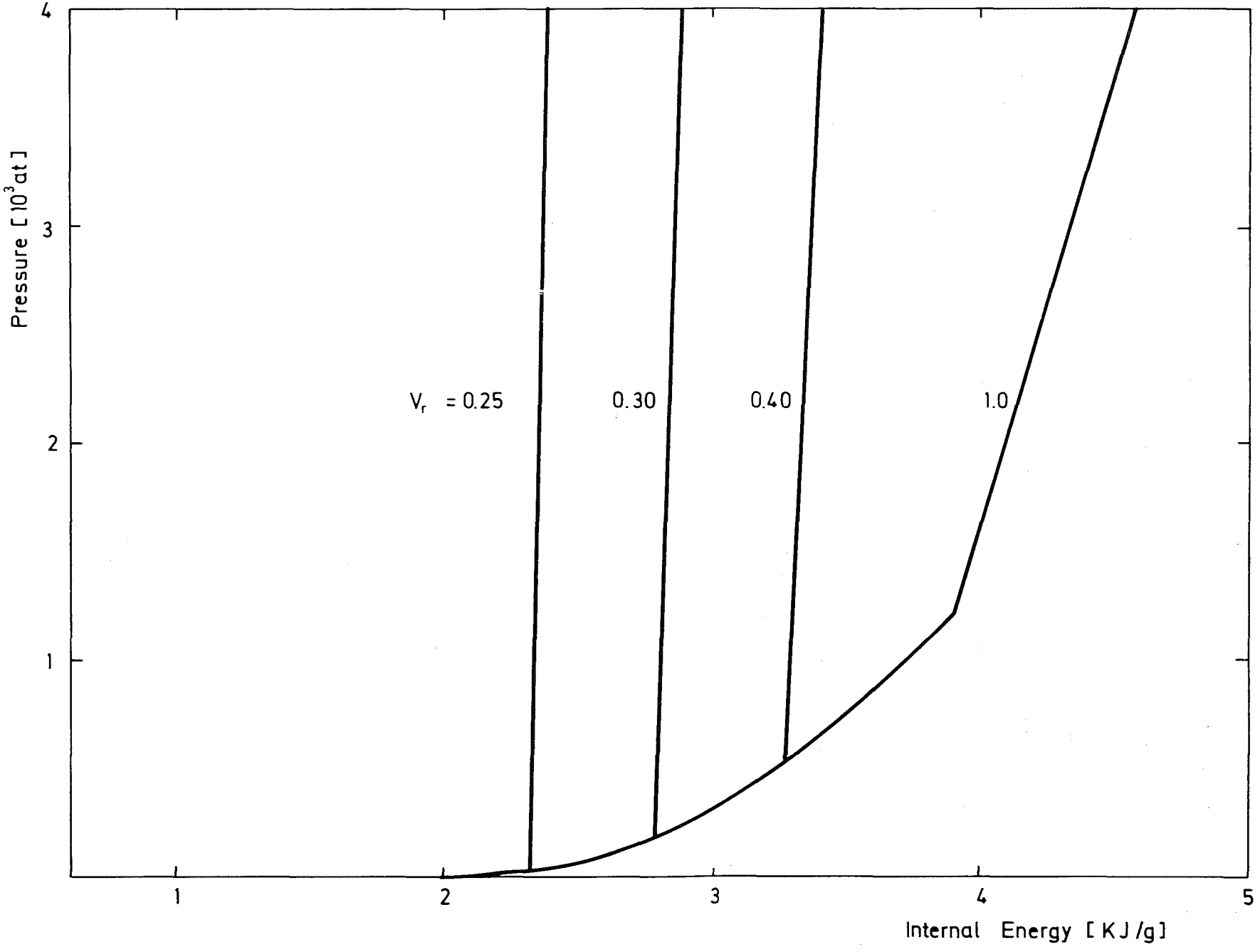


Fig. 3: Equation of State of $UO_2$: Pressure versus Internal Energy ($V_r$ = Reduced Specific Volume)

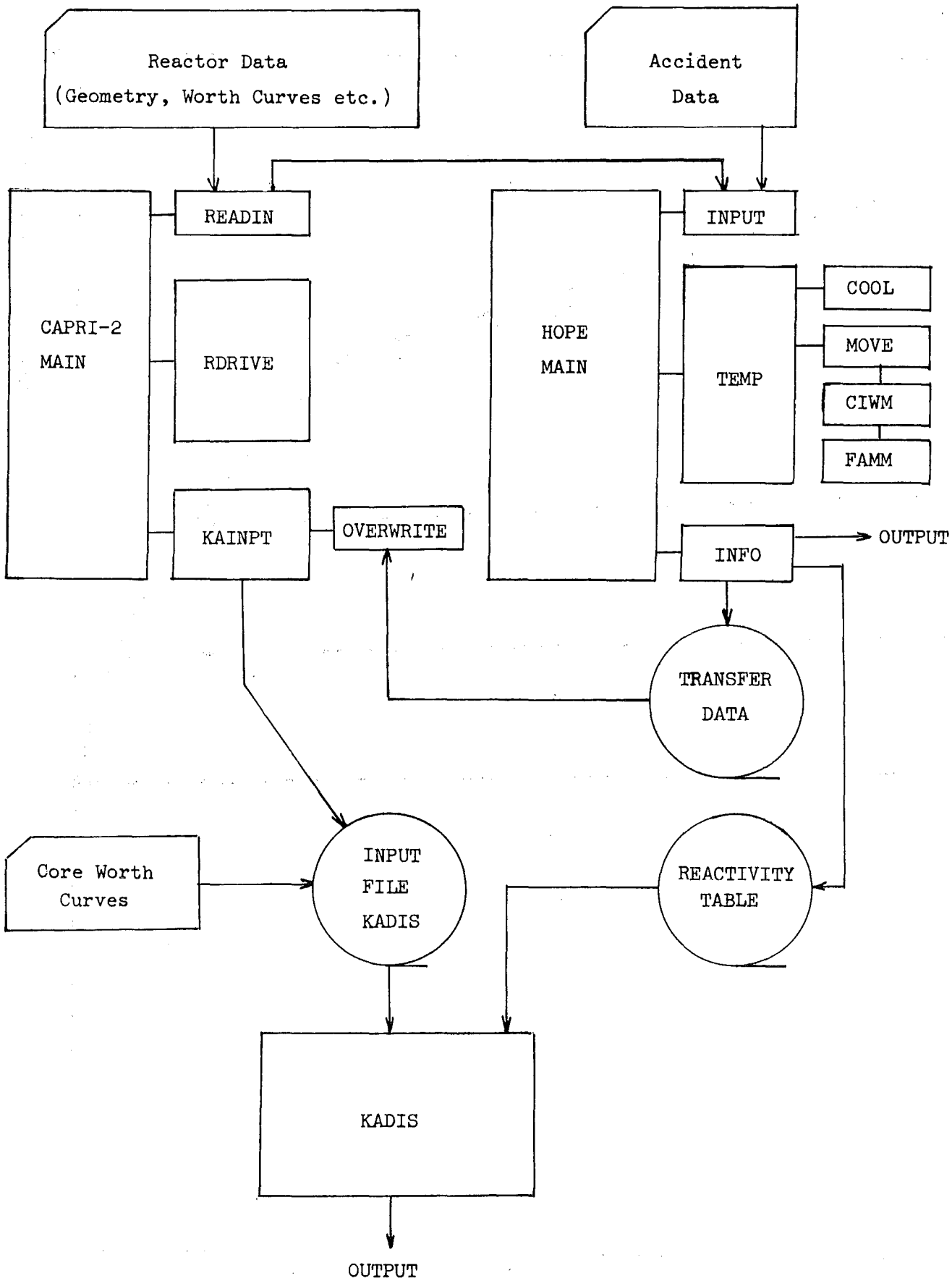


Fig. 4: Code Structure and Data Flow HOPE/CAPRI-2/KADIS

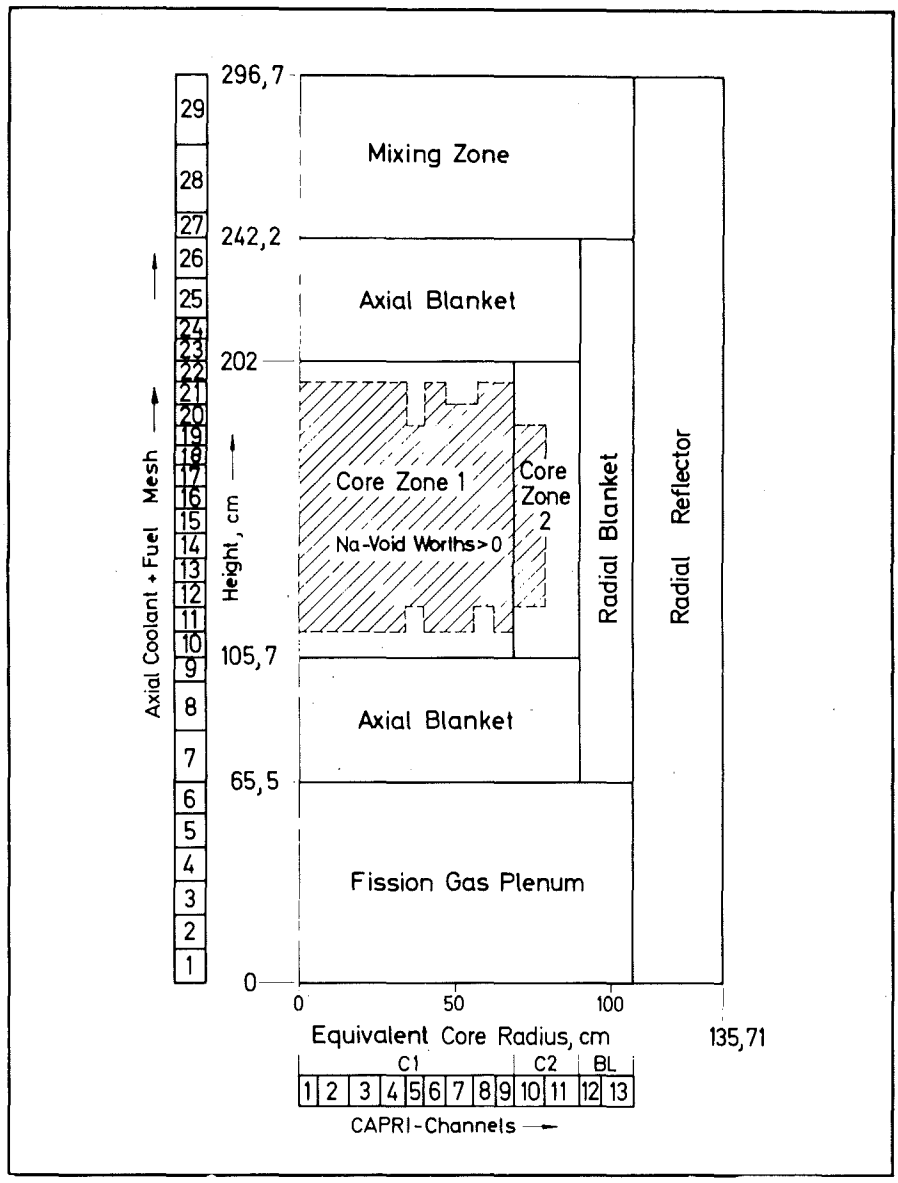


Fig. 5 Setup of the SNR-300 Mark 1 a Core for HCDA Analysis

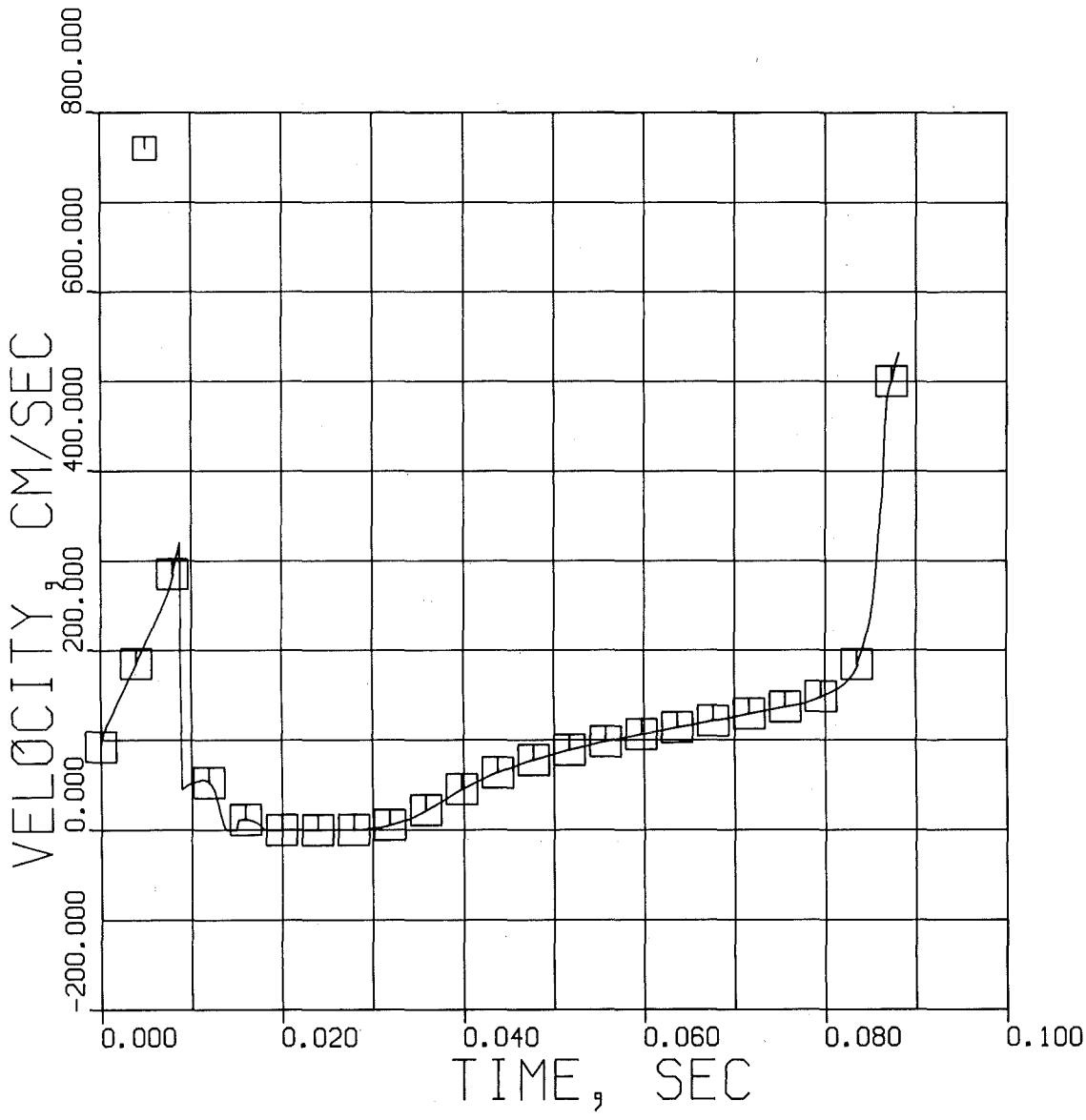


Fig. 6: HOPE Fuel Ejection Velocity in Channel 1. 15 ¢/sec TOP Accident with 30 % Melt Fraction Failure Criterion. (Time after Pin Failure)

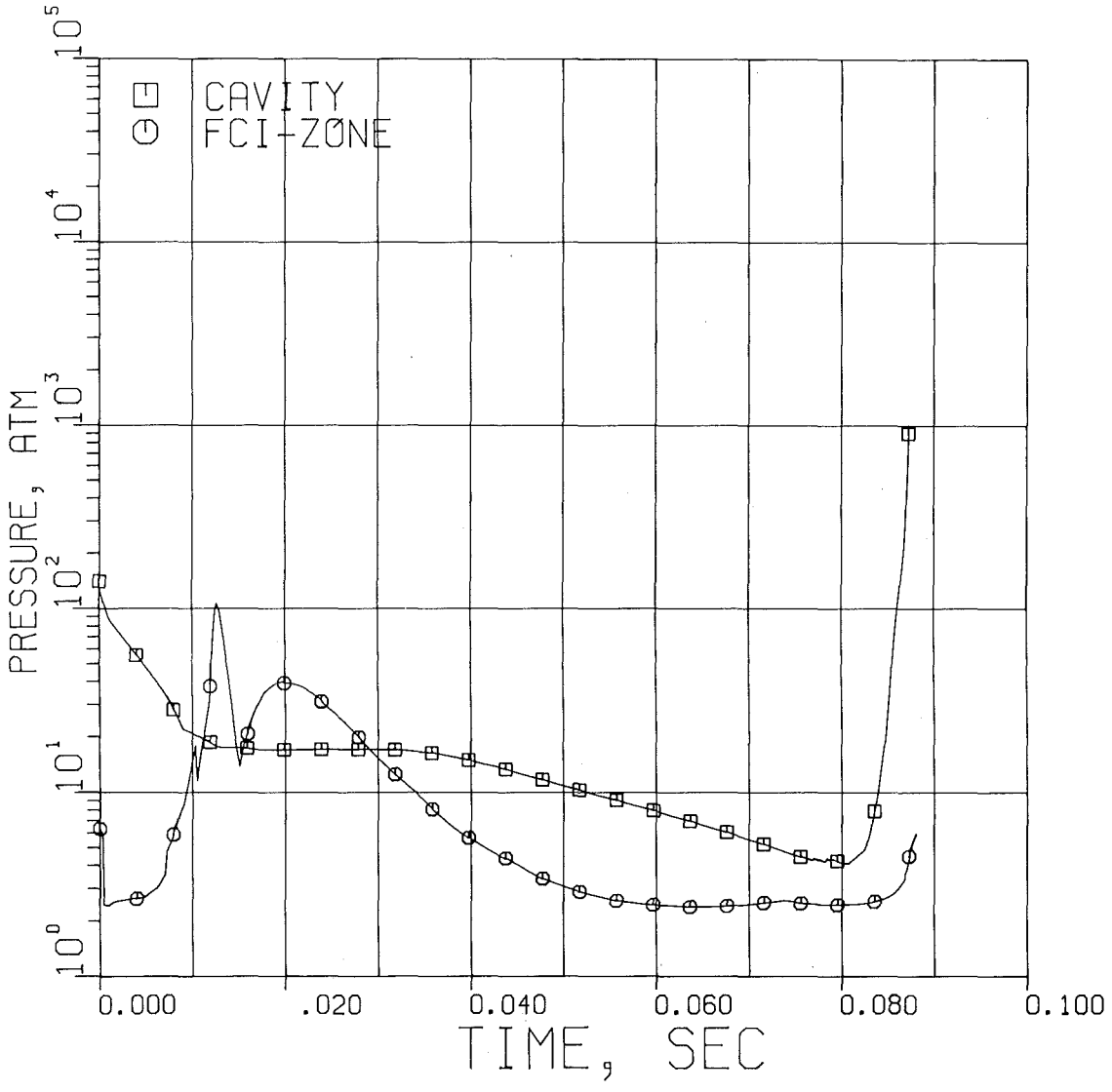


Fig. 7: HOPE Cavity and FCI-Zone Pressure in Channel 1. 15 ¢/sec TOP Accident with 30 % Melt Fraction Failure Criterion. (Time after Pin Failure)

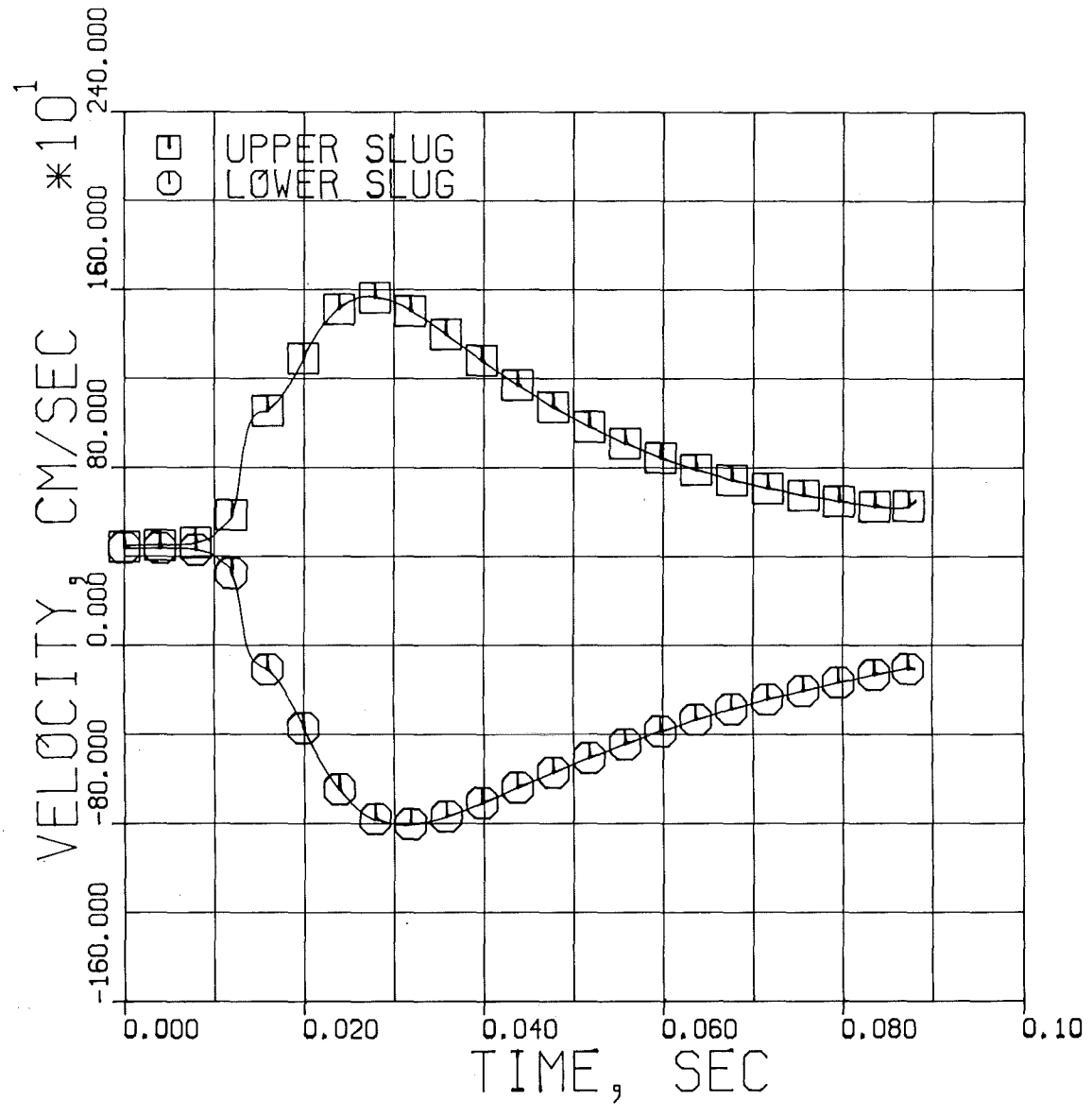


Fig. 8: HOPE Velocity of Interface between FCI-Zone and Upper or Lower Slug (Channel 1). 15 ¢/sec TOP Accident with 30 % Melt Fraction Failure Criterion (Time after Pin Failure)

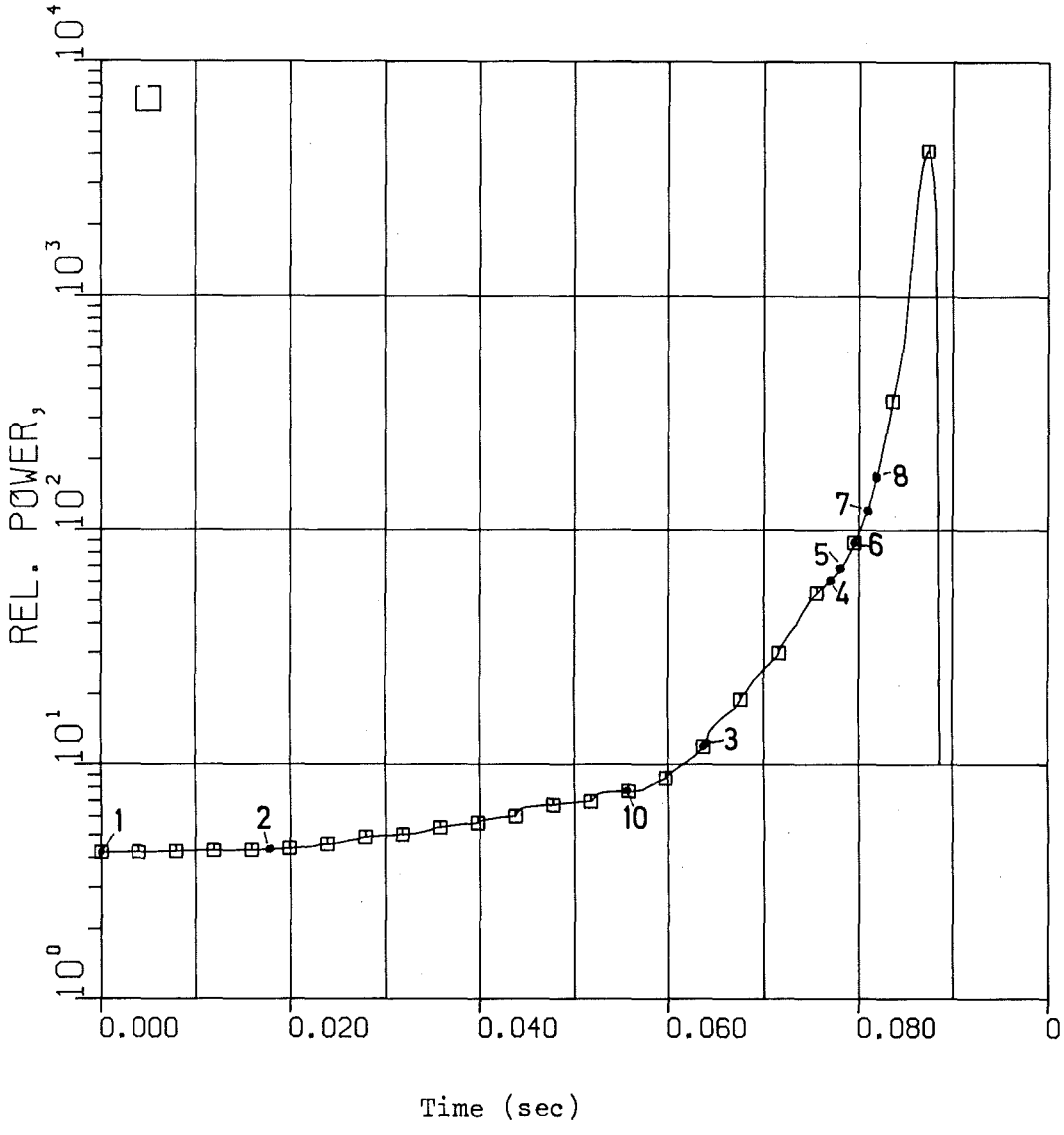


Fig. 9: Normalized Power After First Pin Failure in a 15 ¢/sec TOP Accident with 30 % Melt Fraction Failure Criterion. The Failure Points of the Different Channels are shown.

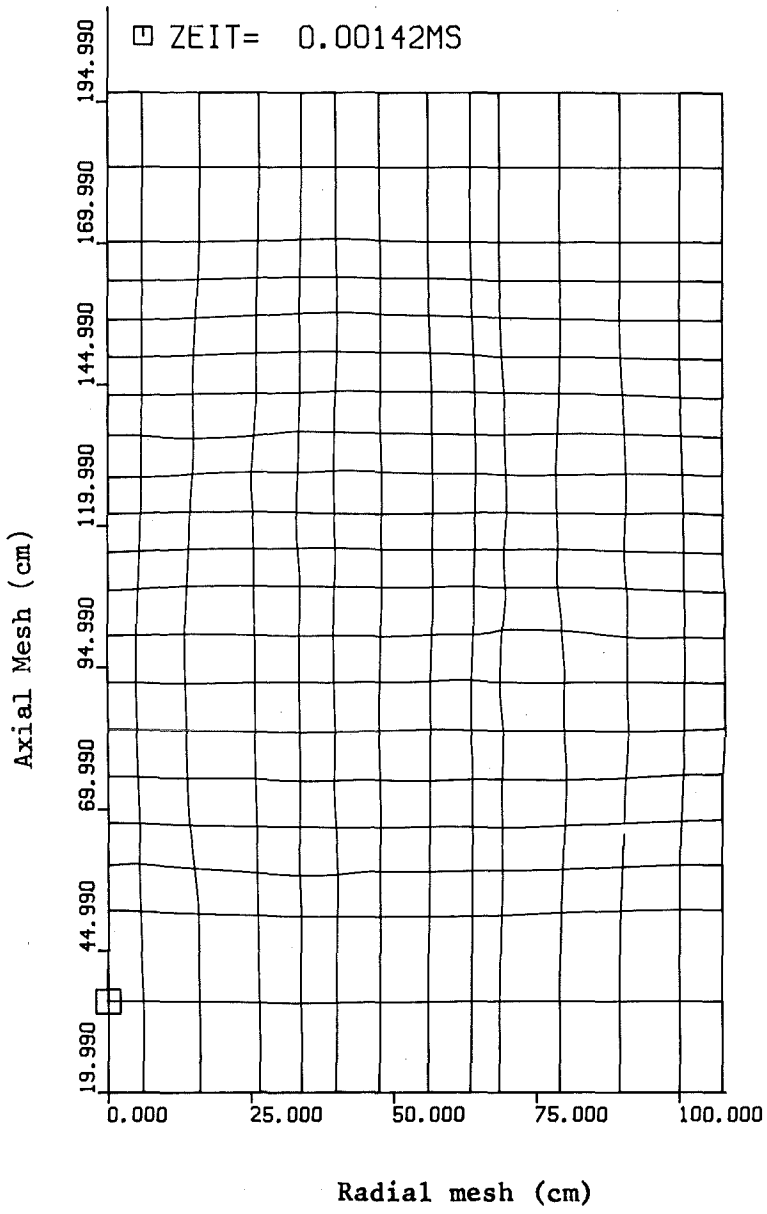


Fig. 10: Distorted Lagrangian Mesh at the End of the Disassembly Calculation (1.42 msec). 15 ¢/sec TOP Accident with 30 % Melt Fraction Failure criterion.

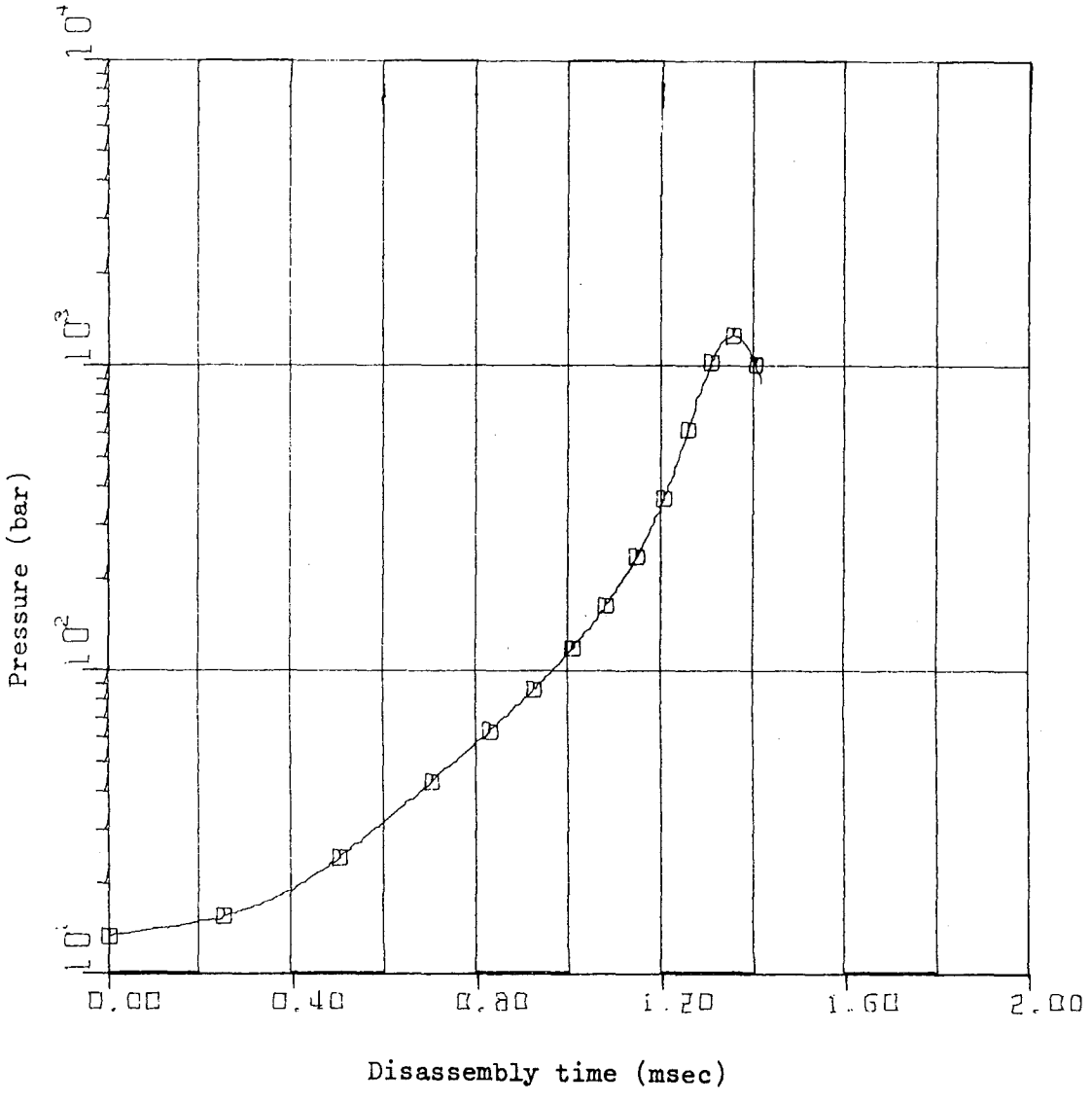


Fig. 11: Pressure History During Core Disassembly (Core Node 7 of Channel 1) 15 ¢/sec TOP Accident with 30 % Melt Fraction Failure Criterion.

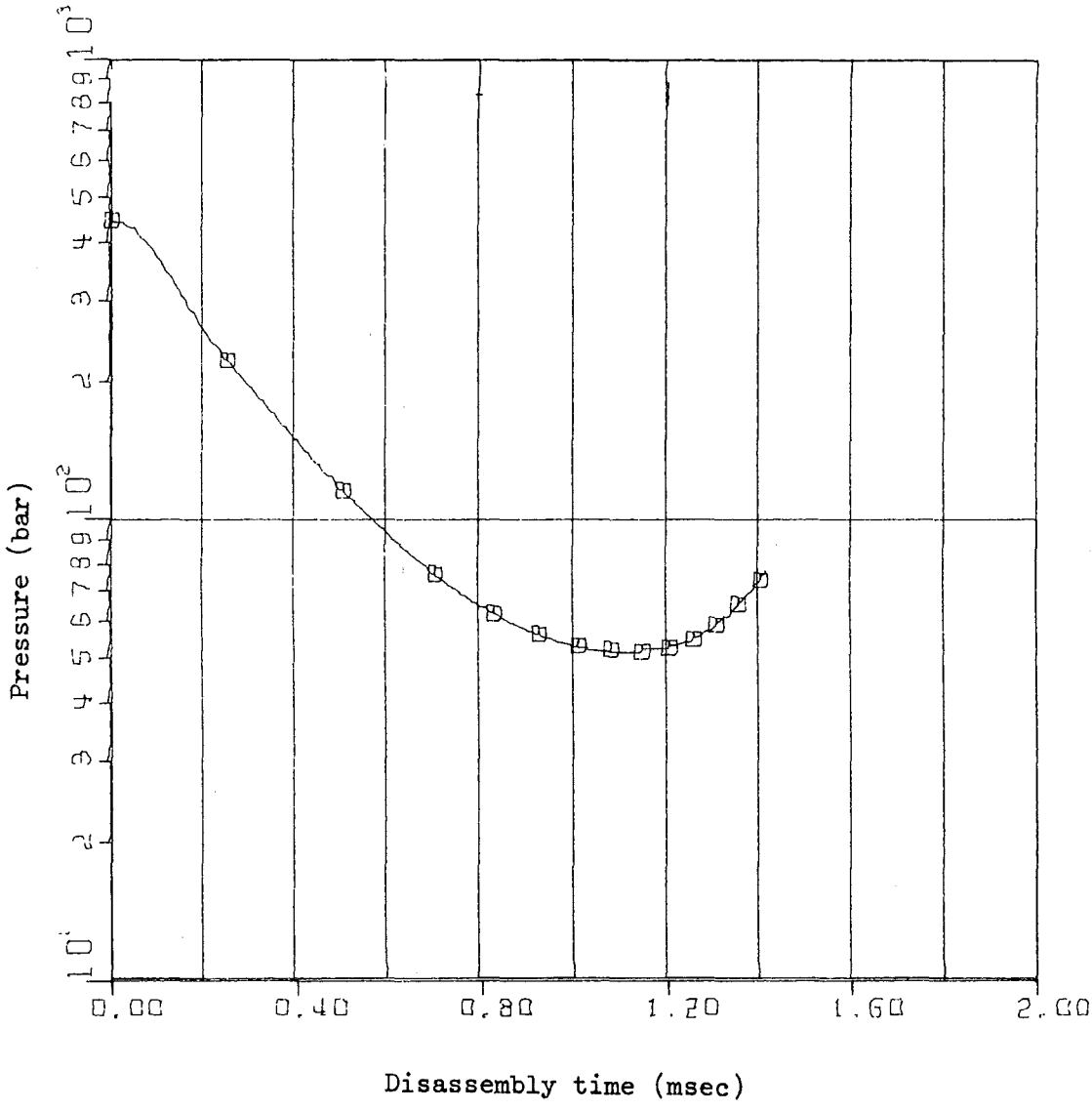


Fig. 12: Pressure History During Core Disassembly (Core Node 7 of Channel 3). 15 ¢/sec TOP Accident with 30 % Melt Fraction Criterion.

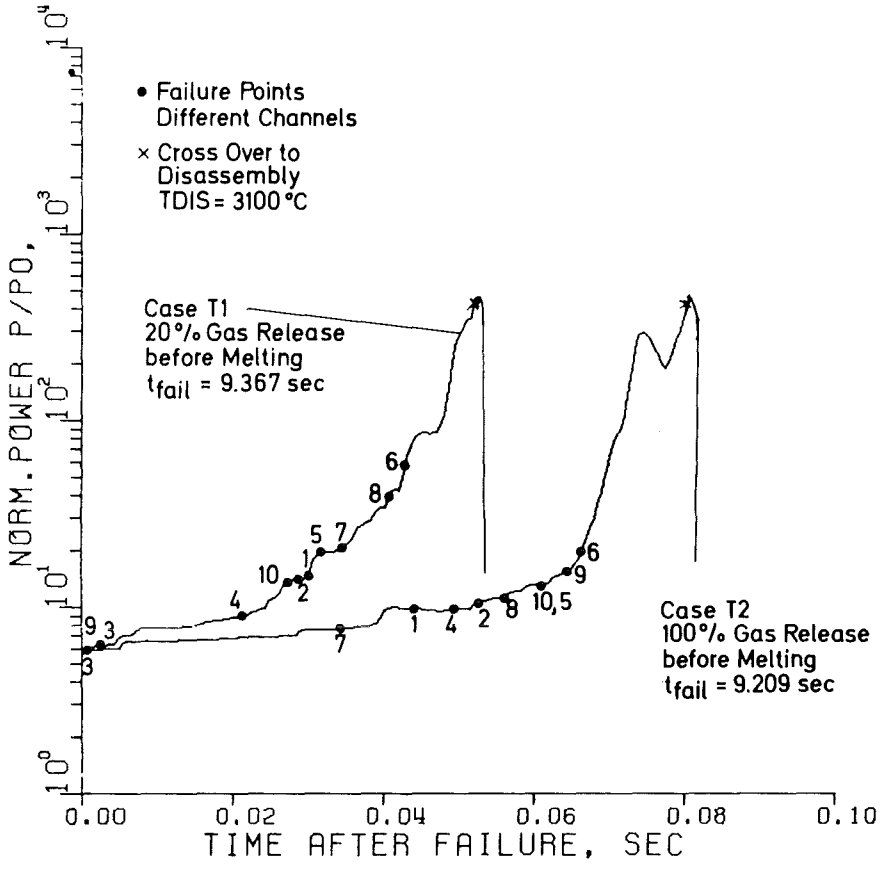


FIG.13: NORMALIZED POWER VS. TIME AFTER 1. FAILURE IN A 0.15 $/SEC TOP ACCIDENT WITH DIFFERENT ASSUMPTIONS FOR RELEASE OF RETAINED FISSION GAS (SNR-300 EOL MARK 1A CORE, BURST STRESS FAILURE CRITERION)